IEEE Access
Multidisciplinary | Rapid Review | Open Access Journal

Received June 20, 2021, accepted August 10, 2021, date of publication August 16, 2021, date of current version August 26, 2021.

Digital Object Identifier 10.1109/ACCESS.2021.3105045

Scenario-Based Investigation on the Effect of Partial Shading Condition Patterns for Different Static Solar Photovoltaic Array Configurations

MOHAMMAD NOR RAFIQ NAZER[1], ABDULFATTAH NOORWALI[2], (Member, IEEE), MOHAMMAD FARIDUN NAIM TAJUDDIN[1], MOHAMMAD ZUBAIR KHAN[3], MOHAMAD AFIQ IZZAT AHMAD TAZALLY[1], JUBAER AHMED[4], (Member, IEEE), THANIKANTI SUDHAKAR BABU[5], (Senior Member, IEEE), NUR HAFIZAH GHAZALI[6], (Member, IEEE), CHINMAY CHAKRABORTY[7], AND NALLAPANENI MANOJ KUMAR[8], (Member, IEEE)

[1]Faculty of Electrical Engineering Technology, Universiti Malaysia Perlis at Pauh Putra, Arau, Perlis 02600, Malaysia
[2]Electrical Engineering Department, Umm Al-Qura University, Makkah 21961, Saudi Arabia
[3]Department of Computer Science and Information, Taibah University, Madinah, Saudi Arabia
[4]Faculty of Engineering, Computing and Science, Swinburne University of Technology Sarawak, Kuching 93350, Malaysia
[5]Department of Electrical and Electronics Engineering, Chaitanya Bharathi Institute of Technology (CBIT), Hyderabad 500075, India
[6]Faculty of Electronic Engineering Technology, Universiti Malaysia Perlis at Pauh Putra, Arau, Perlis 02600, Malaysia
[7]Department of Electronics and Communication Engineering, Birla Institute of Technology Mesra, Jharkhand 835215, India
[8]School of Energy and Environment, City University of Hong Kong, Hong Kong

Corresponding authors: Thanikanti Sudhakar Babu (sudhakarbabu66@gmail.com) and Nallapaneni Manoj Kumar (mnallapan2-c@my.cityu.edu.hk)

This work was supported by the Ministry of Education (MOE) Malaysia through the Fundamental Research Grant Scheme (FRGS) under Grant FRGS/1/2018/TK07/UNIMAP/02/1.

ABSTRACT This paper presents an in-depth analysis and investigation on the performance of static photovoltaic (PV) array configurations subjected to various partial shading conditions (PSCs). Under PSCs, the electrical characteristics of the PV modules are critically monitored and reasons for their behavioral changes are highlighted. By doing so, this study aims to improve the efficiency of PV systems by minimizing mismatch losses and determining the optimum array configuration which is characterized by the highest maximum power and lowest relative losses under PSCs. Besides, this study complements and carries forward the previous studies through the detailed analysis of each configuration subjected to various practically probable PSCs. Three different PV array sizes (5×4, 5×5, and 3×10) are used to analyze the results and performance under considered shading scenarios. MATLAB/Simulink platform is used to model and simulate the PV array using the single diode (5-parameters) model. In-depth analysis of current flow across cross-ties and bypass diodes activation shows that the diagonal shading pattern leads to lower power loss (PL). Besides, the Total Cross-Tied (TCT) configuration demonstrates superior performance under most of the PSCs compared to other configurations. These results provide valuable information about the performance of PV array which may lead to better estimation and prediction of global maximum power (GMP) generation of a PV system.

INDEX TERMS Single diode solar cell model, photovoltaic array, PV reconfiguration schemes, total cross tied configuration, performance of static photovoltaic array, partial shading conditions, energy loss.

I. INTRODUCTION

Over the last decades, power generation has shifted heavily towards renewable sources due to environmental concerns and the increasing efficiency of renewable technologies. PV systems have offered good results and have been largely integrated into the power networks of many countries. Development and improvements in semiconductor technology have further boosted the popularity of PV systems as a reliable renewable source. Researchers have targeted other

The associate editor coordinating the review of this manuscript and approving it for publication was Jenny Mahoney.

ways such as sun tracker, PV array reconfigurations, and maximum power point tracker to improve the efficiency and reach optimal performance of PV systems [1]. One of the major factors that reduce the conversion efficiency of PV systems is PSCs. Studies carried out to show that PSCs can be considered as main cause of power losses from 10-70% of the system yield [2], [3]. The broad range is due to the wide range of shading patterns and intensity of the shading conditions. PSCs are most prominent in building integrated PV (BIPV) systems where shading patterns occur due to nearby, and often taller, building structures, utility towers, trees, and other structures in proximity of the installed PV systems [4]. Problem is often difficult to solve since many of the shading structures would appear after the installation, e.g. construction of a taller building. As a result, these obstructions cannot be countered during installation and BIPV systems suffer from low efficiency for the latter portion of their lifetime [5], [6].

In larger PV installations, such as a power generation plant, the issue of PSCs rises from a passing clouds. Due to the moving clouds, only a few portions of the PV array are subjected to shading while others receive a uniform and higher irradiation level. Moreover, this shading is dynamic and practically impossible to predict in advance. Other factors that lead to PSCs include physical damage and aging to PV module (such as cracks) and animal residues or other forms of remains (leaves, dust, debris) on PV module that have not been removed on time [7]. Due to its impact on power generation, the phenomenon of PSCs has been studied thoroughly in literature and the problem is well clarified [8]. During PSCs, shade PV cells turned into a load which can cause the PV cell to raise the temperature and affected the whole PV panel. This phenomenon is called as hot spot effect. The PV cell would become reverse biased during the generation of current through the PV module. To counter that, several researchers had proposed to connect the PV cell parallel with bypass diodes. This solution helped to bypass the current produce by non-shaded PV cells from passing through shaded PV cells [9]–[11]. However, such bypass diode activation results in the generation of multiple maximum power points (MPP) on the Power-Voltage (P-V) curve under PSCs [12]–[14]. Such a phenomenon causes tracking problems for the MPP Tracker (MPPT) that may detect Local Maximum Power Point (LMPP) instead of Global Maximum Power Point (GMPP) [13], [15]. The PSCs will lead power loss, waste of energy, downturn the efficiency of PV, and alter the payback period to the PV investor. The approaches to minimize the negative effects of PSCs, effectiveness, and cost trade-off. However, as mentioned before, PSCs are often impossible to predict and account for, much of the research focuses on maximizing the energy yield of the PV system under PSCs.

In general, the issue of reduced energy yield is countered by either adapting the MPPT algorithm by governing the converter(s) used in the system architecture [16] or by changing the array configuration of the PV system from series-parallel (SP) to bridge-linked (BL), to Honey Comb (HC) or to total cross-tied (TCT), or a different array configuration [17], [18]. The summary from the analysis is stated in 1. The second approach i.e. the modification of array configuration has been taken by many researchers who have developed models to study and analyse different configurations of PV arrays and how each configuration responds to PSCs. A generalized MATLAB program was developed by Ramaphraba and Mathur to analyse and compare array configurations for random shading pattern and to find a configuration with the lowest sensitivity to power loss under PSCs [19]. The results indicated that TCT configuration was superior for symmetrical array sizes while HC configuration was optimal for asymmetrical array sizes [20]. Belhachat and Larbes analysed the advantages and limitations on series (S), parallel (P), SP, TCT, BL, and HC in their work. The work also provided the detail on power loss for all configurations [17]. However, this work does not state the detail on the behaviour of electrical power flow in each configuration.

Wang and Hsu studied the electrical performance of PV modules with S, SP, TCT, BL, and HC array configuration. They used the Newton-Raphson and piecewise linear parallel branches (PLPB) model methods for PV cells and determined that TCT configuration yielded the maximum power value with both methods. TCT was followed by BL and HC array configurations for the shading pattern studied. Again only one PSCs pattern was used and therefore the results cannot be accepted for a general case [21].

Other approaches that had been implemented and studied by previous researchers are the Sudoku configuration and Zig-Zag configuration such as presented by [22], [23]. Basically, Zig-Zag and Sudoku configurations are based on puzzle game theory for the physical relocation of PV panels under different PSCs. In addition to static reconfirmation methods dynamic or electrical array reconfiguration methods were proposed by various researchers. With excellent behaviour of meta-heuristic algorithms reconfiguration of PV systems were developed via population based algorithms [24], artificial ecosystem [25], grey wolf optimizer [26]. Authors in [27] also proposed the Sudoku configuration, the applied method involved modification of the modules' arrangement by relocating the panel from its original location to a new location in the same column. The transportation process is executed without changing the electrical connection. The node current under PSCs is expected to be increased by applying this approach, hence, as the result shows the GMPP of the proposed PV array relocation technique is significantly larger compared to TCT. Even though these techniques significantly improvised the PV arrays performance under numerous PSCs, however, these techniques possess consequential limitations to be applied in real-life such as imprudent wiring connection due to the physical relocation of PV panels, laborious task suffers, and for Sudoku technique it can be only applied to arrays with even number of array size. Further, to verify the implementation of array reconfirmation methods for large scale PV system an innovative method for a PV array of 16×16 and 25×25 are proposed in [28].

In [29], the authors have introduced Symmetric matrix based shade dispersion capability to enhance PV array performance. Three realistic shading scenarios are considered and a comprehensive study is carried out to show higher GMPP compared to Shape-do-Ku, novel TCT (NTCT) an conventional TCT configurations. Effect of bypass diode is investigated during the PSCs on a SP configured PV array. Various connecting of bypass diode topologies are adopted and compared under four shading scenarios in terms of GMPP location and improved FF etc.

Meanwhile, authors in [30] presented in their paper about the analysis and comparison of the PV array configurations including S, SP, BL, HC, and TCT under six different PSCs. Their comprehensive study implemented a symmetrical array size only which is 6 × 6. Their study shows that the TCT configuration outperforms the other configurations in terms of lowest mismatch lost and fill factor, highest efficiency, and highest maximum power output under all of the conditions tested by the authors. However, their paper does not explain in detail the characteristic of components in the PV array configurations under certain PSC such as the characteristic of bypass diode for the shaded and unshaded modules, and also the characteristic of P-V curve under certain PSCs.. Furthermore, their study only used a symmetrical array size under six conditions. As a result, if the array size is unsymmetrical, such as 3 × 5, the other configurations may outperform the TCT interconnection under certain PSCs. Moreover, there are millions of possibilities PSCs patterns might occur for different array sizes. Hence, six conditions is not enough to compliment that the TCT scheme outperforms the other configurations. Another paper that discussed the same topic in [31] focuses on the seven parameter variations for multiple PV arrays topologies under different PSC and also faulty PV scenarios. The seven parameters utilized by the authors for their analysis and investigation are short circuit current (I_{SC}), open voltage circuit (V_{OC}), current at maximum power point (IMPP), the voltage at maximum power point (VMPP), series resistance (RS), FF and thermal voltage (V_{te}) to detect and analyse the PV arrays with faulty PV panels under different PSC for future generic MPPT learning algorithm improvement, instead of predicting the PSC. Their paper is undeniably a good reference for MPPT algorithm improvement since their paper provided a detailed analysis by using all of the indicators and considering the faulty PV panels. However, their paper applied an unsymmetrical array size only which is 6 × 4 for all of the topologies. In addition, the authors tested the PV arrays interconnection under 18 various PSC for each topology, however, in-depth analysis wasn't provided.

Furthermore, their study only used a symmetrical array size under six conditions. As a result, if the array size is unsymmetrical, such as 3 × 5, the other configurations may outperform the TCT interconnection under certain PSCs. The analyses presented in this paper encompass multiple practical configurations and their response to several possible and realistic shading patterns. A study in such detail and with multiple configurations, array sizes and shading patterns has not been presented in previous researches. In this paper, the detailed analyses of static PV array configurations i.e. series (S), parallel (P), series-parallel (SP), bridge-link (BL), honeycomb (HC), and total-cross tied (TCT) configurations under possible patterns of shading. Furthermore, a comprehensive analysis of the current distribution for TCT configuration is also done and activation of bypass diodes and linkages during PSCs is also discussed. Firstly, PV array configuration with different sizes is modelled and then each configuration is analysed under different shading patterns. The output power and the power loss of different configurations under different PSC patterns have been compared. The optimised PV configuration has been selected based on lower power loss under different shading patterns. Besides, the optimised PV configuration can contribute as the topology for PV array reconfiguration (PVAR). The result from the analysis of bypass diodes and the activation of PV modules can help in developing the maximum power point tracking (MPPT). This process determines the optimal configuration under a given PSCs. This optimal configuration can be exploited to provide high yield even under PSCs and improve the efficiency of the overall PV system.

To facilitate a comprehensive reading experience, this paper is structured in the following way. Section II describes the modelling technique of a PV module, partial shading effect and different types of PV array configurations. It should be noted that, in this work, the PV module available in the Simulink library is used. This model is available to every Simulink user, thus, our experiments can be reproduced and verified by any party. Section III, detailed the effect of partial shading on the various PV configuration by describing the behavior of bypass diodes, flow of the current and how multiple peaks are generated in different scenarios. In section IV, comparative analysis is carried out using simulation results and a thorough investigation is presented. Finally, the conclusions are drawn in section V.

II. SYSTEM DESCRIPTIONS

A. SINGLE DIODE PV MODEL

To model the PV array characteristics, the single diode model of PV module is used since it provides a good trade-off between simplicity of the model and the accuracy. The single diode model presented by authors [32], [33] provides a good qualitative prediction of PSC and mismatch effects. Additionally, it is also impractical to compute a very accurate model for each cell in a large PV system due to inherent variations in cell parameters. It is notable that, the default model in MATLAB/Simulink is also based on the single diode model as presented in Fig. 1(a) and Fig. 1(b). Therefore, the single diode model of PV cell shown in Fig. 1(c) serves as a suitable candidate for this study. Since, the MATLAB default model is used in this study, our simulation results can be reproduced or verified by any other Matlab user with ease.

TABLE 1. Analysis of PV configurations.

Configuration	Advantages	Limitation
Series (S)	• Using less wire. • Configuration not complicated.	• Low current flow through configuration. • Produce high voltage at output terminal. • Low output power under partial shading condition. • High current flow through configuration.
Parallel (P)	• Configuration not complicated. • Produce single peak of power-voltage (P-V) curve under uniform irradiance and partial shading.	• High current flow through configuration. • Produce high voltage at output terminal. • High current flow may damage the configuration and other appliances.
Series-parallel (SP)	• Common configuration used in PV industries. • Produced balanced current and voltage compared to S and P configurations.	• More power losses compared to TCT under partial shading. • Multiple peak produce on P-V curve under partial shading conditions.
Bridge-Link (BL)	• Produced high maximum output power compared to SP and HC under certain shading patterns. • Provide more paths for current to flow through configuration.	• Configuration is complex. • More wire used. • High wiring loss • Produced low maximum output power under partial shading conditions compared to TCT. • Produced low maximum output power under partial shading conditions compared to TCT.
Honeycomb (HC)	• Provide more paths for current to flow through configuration. • Produced high maximum output power compared to SP under certain shading patterns.	• High wiring loss. • Configuration is complex. • Low maximum output power under partial shading conditions compared to TCT and HC. • Multiple peak produce on P-V curve under partial shading conditions.
Total-cross tied (TCT)	• Produced high maximum output power compared to other configurations under most shading patterns. • Provide more paths for current to flow through configuration. • Less power losses under most shading patterns.	• Very high wiring loss. • More wire used.

The electrical behaviour of PV cell is related to the module voltage via Eq. 1.

$$I_{pv} = I_{ph} - I_0 \left\{ exp\left(\frac{V_{pv} + I_{pv}R_s}{a_1\ V_t} \right) - 1 \right\} - \frac{V_{pv} + I_{pv}R_s}{R_p} \quad (1)$$

where I_{ph}: light generated current, I_{pv}: current generated by incident light, I_0: reverse saturation current, R_s: series resistance, R_{sh}: parallel resistance, a: diode ideality constant, V_T: thermal voltage of the PV module with NS cells connected in series (NskT/q), q: electron charge ($1.60217646 \times 10^{19}$), k: Boltzmann constant (1.3806503×10^{23} J/K).

The PV module can be built by scaling the thermal voltage according to series connected PV cells NS in a module. Besides, the light generated current I_{ph} is depends on short circuit current in standard test condition ISC,STC and the irradiance experienced by the surface of PV module G as

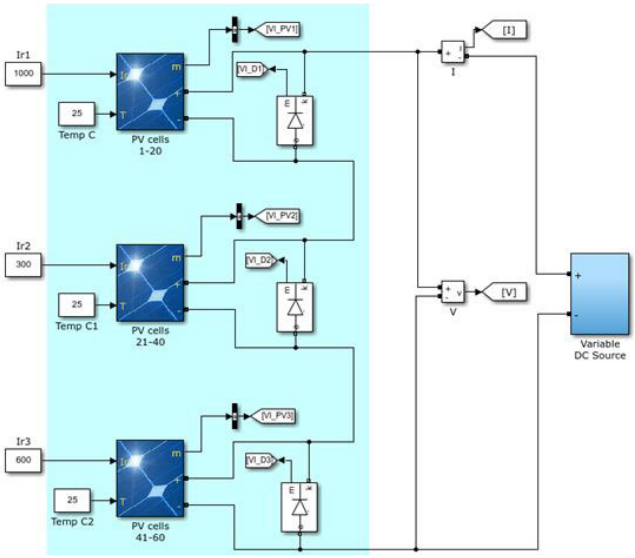

(a)

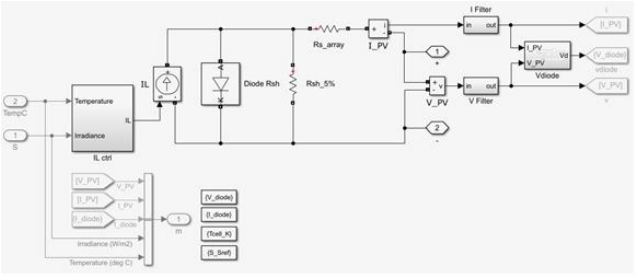

(b)

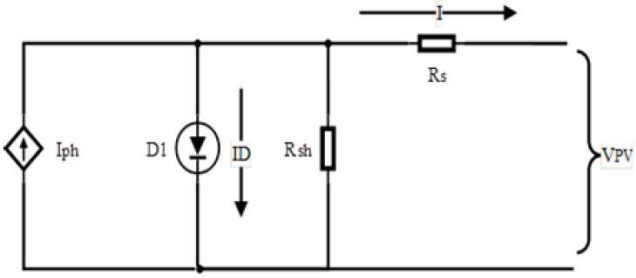

(c)

FIGURE 1. Basic connections schemes, (a) Default Simulink model, (b) Modeling of a PV module in Simulink using single diode model and (c) Theoretical single diode PV cell equivalent circuit.

stated in Eq. (2)

$$I_{ph} = (I_{SC,STC} + K_i \Delta T)\frac{G}{G_{STC}} \tag{2}$$

where K_i is the temperature coefficient of the short circuit current and $\Delta T = T - T_{STC}$, where T is the temperature of PV module. The conditions that been set for STC are $T_{STC} = 25°C$, $G_{STC} = 1000\ W/m^2$, and air mass (AM) = 1.5. On the other hand, the reverse saturation current is extracted from open circuit voltage in STC $V_{OC,STC}$ and temperature coefficient of open circuit voltage K_v as shown in Eq. (3)

$$I_0 = \frac{I_{SC,STC} + k_V \Delta T}{e^{(\frac{V_{OC,STC} + k_V \Delta}{aV_T})} - 1} \tag{3}$$

The parameters of the PV cell used in this paper are based on the National Renewable Energy Laboratory (NREL) database. For this study, API156P-230 module manufactured by Advance Solar Hydro Wind Power is selected. Its electrical parameters are tabulated in Table 2.

TABLE 2. Electrical characteristics of API156P-230 module.

Parameter	Value
Maximum Power	230 W
Cells per module (Ncell)	60
Open Circuit Voltage (V_{OC})	60
Short Circuit Current (I_{SC})	8.19 A
Voltage at Maximum Point (V_{MP})	30 V
Current at Maximum Point (I_{MP})	7.66 A
Temperature coefficient V_{OC}	-0.356 %/^{0}C
Temperature coefficient I_{SC}	0.07 %/^{0}C

B. PV ARRAY CONFIGURATIONS

For a PV system, the interconnection scheme describes the interconnections of the PV modules in the array. For S configuration, a few PV modules are connected in series. Meanwhile, a few PV modules are connected in parallel to form P configuration. Series of panels are connected in a string, and multiple such strings are connected in parallel to form the SP scheme or configuration. The SP configuration is the most popular scheme due to its simplicity and low cost. However, this scheme is highly sensitive to PSC conditions and experiences heavy power losses. To mitigate that limitation other configurations are proposed i.e. BL, HC and TCT where the energy yield is better than SP configuration especially under PS condition. BL is the connection of a few groups containing 2 PV modules per group connected by cross-ties (CT) and HC is mocking the beehive pattern as the columns are connected with CT. On the other hand, parallel connected PV modules are connected in series and CT is connected across each junction in TCT. The S, P, SP, BL, HC and TCT interconnection schemes are shown in Fig. 2 respectively with a 5 × 4 PV array.

C. UTILIZATION OF BYPASS DIODE TO REDUCE THE EFFECT OF PARTIAL SHADING

During partial shading occurrences, certain PV modules in the PV array are shaded due to dust, tree, passing clouds or chimney. The current from non-shaded PV modules are dumped into shaded PV modules inside the array under partial shading condition as illustrated in Fig. 3(a). This phenomenon will lead to overheating and damage the shaded PV modules inside the array [34]. To counteract this detrimental effect, bypass diodes are usually connected in anti-parallel with PV modules in an array.

It creates new path for current produced by non-shaded PV modules to flow across the array without affecting the shaded modules, thus the energy yield by the PV array can

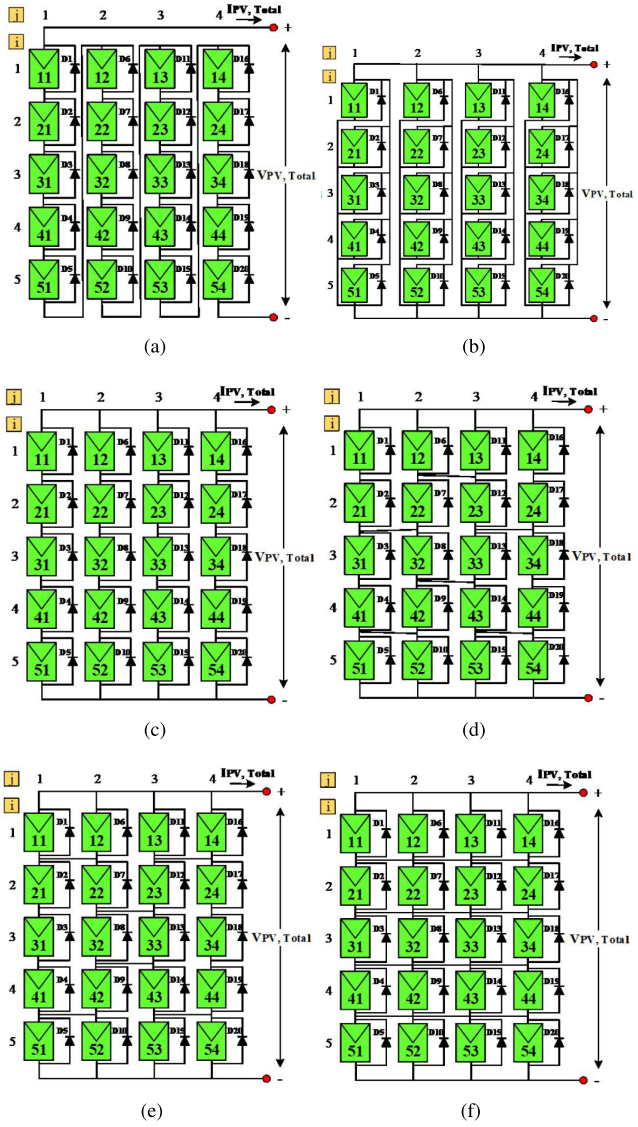

FIGURE 2. Types of interconnection schemes: (a) series, (b) parallel, (c) series parallel, (d) bridge linked, (e) honeycomb, (f) total cross tied.

be improved during -PSCs as shown in Fig. 3(b) [35]–[37]. The switching state of PV module and the bypass diodes for different PV configurations under different patterns of the partial shading are provided in Supplementary Information.

Fig. 4 shows 3 × 1 PV array connected in series subjected to a) non-shaded condition b) partially shaded condition without bypass diodes and c) partially shaded condition with bypass diode.

It can be seen from the generated PV curve of these three conditions shown in Fig. 5 that non-shaded PV array is producing more power as compared to shaded PV array. Meanwhile, for partially shaded PV array the one without bypass produced the lowest output power because the current in the string is limited by the affected PV module. Therefore, bypass diodes have minimized the effect of partial shading on the performance of PV array.

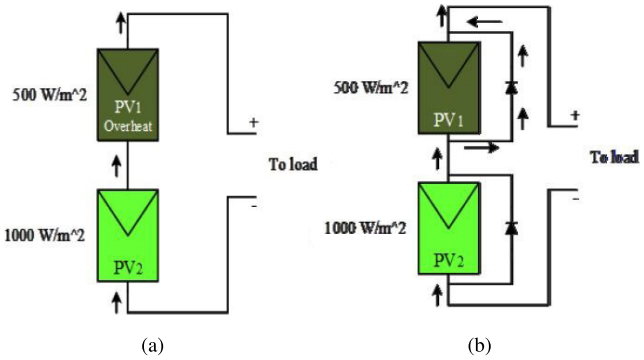

FIGURE 3. Current flow under PSC: (a) without bypass diode, (b) with bypass diode.

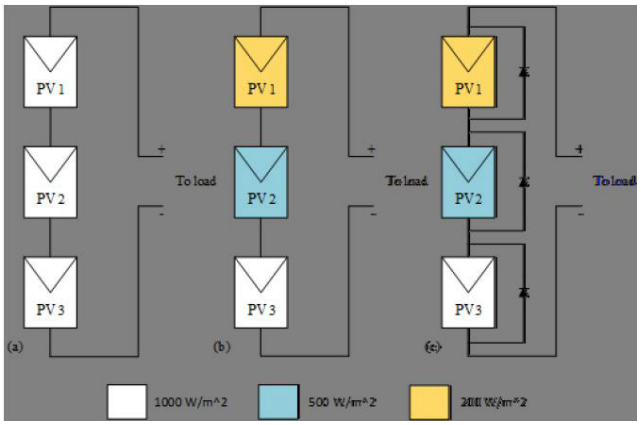

FIGURE 4. Effect of bypass diode: (a) non-shaded condition; (b) partially shaded condition without bypass diodes; (c) partially shaded condition with bypass diode.

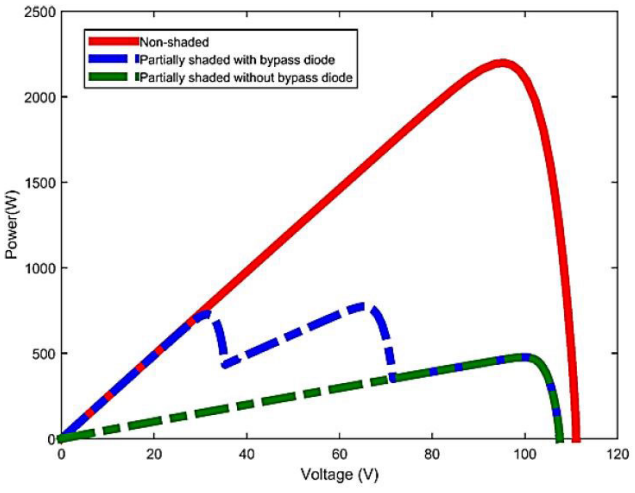

FIGURE 5. The PV curves of non-shaded, partially shaded with bypass diodes, and partially shaded without bypass diodes.

III. DETAIL ANALYSES ON STATIC PV ARRAY CONFIGURATIONS DURING PS CONDITION

To analyse the characteristics and understand the working principle of S, P, SP, BL, HC and TCT configurations during

TABLE 3. Shading pattern of PV array.

PV1 1000 W/m^2	PV6 1000 W/m^2	PV11 1000 W/m^2	PV16 1000 W/m^2
PV2 1000 W/m^2	PV7 800 W/m^2	PV12 800 W/m^2	PV17 1000 W/m^2
PV3 1000 W/m^2	PV8 600 W/m^2	PV13 600 W/m^2	PV18 1000 W/m^2
PV4 1000 W/m^2	PV9 400 W/m^2	PV14 400 W/m^2	PV19 1000 W/m^2
PV5 1000 W/m^2	PV10 1000 W/m^2	PV15 1000 W/m^2	PV20 1000 W/m^2

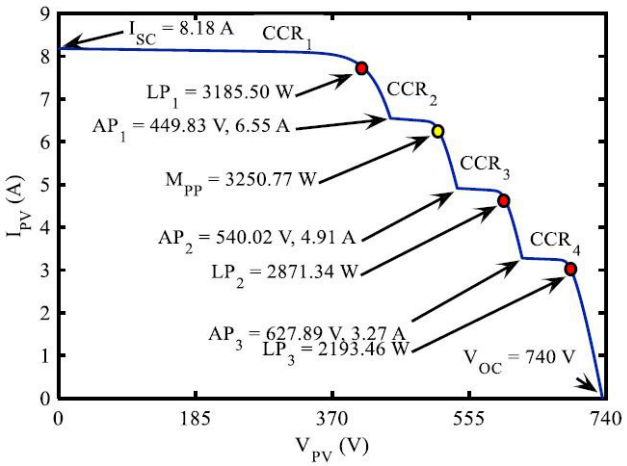

FIGURE 6. IV curve of S.

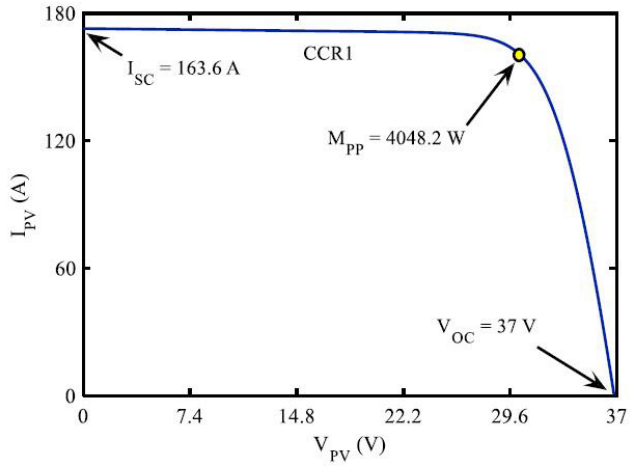

FIGURE 7. IV curve of P.

PSC occurrence, the array of 5 × 4 size are tested with the shading pattern shown in Table 3. All configurations are imposed with the same shading pattern and for simplicity of the analyses the temperature of all modules is assumed to be fixed at 250°C. For uniform irradiance condition at STC, the maximum available power from the array is 4.6 kW.

The results of the IV and PV curves for S, P, SP, BL, HC and TCT configurations are shown in Fig. 6 to 14 and the global peak value for each configuration is presented in Table 4.

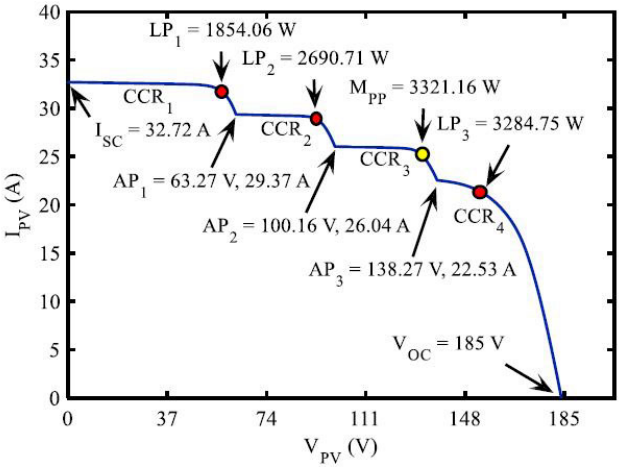

FIGURE 8. IV curve of SP.

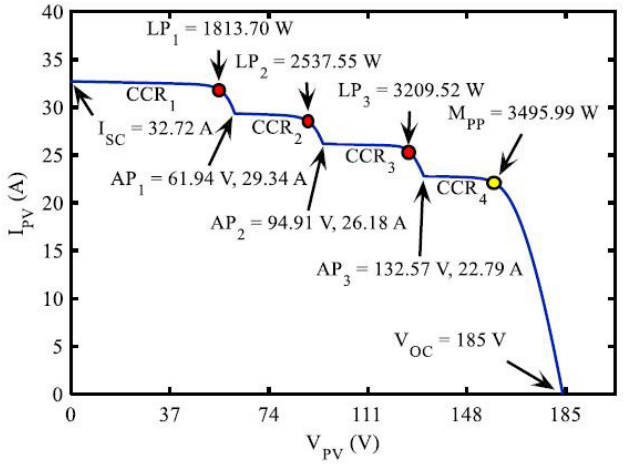

FIGURE 9. IV curve of BL.

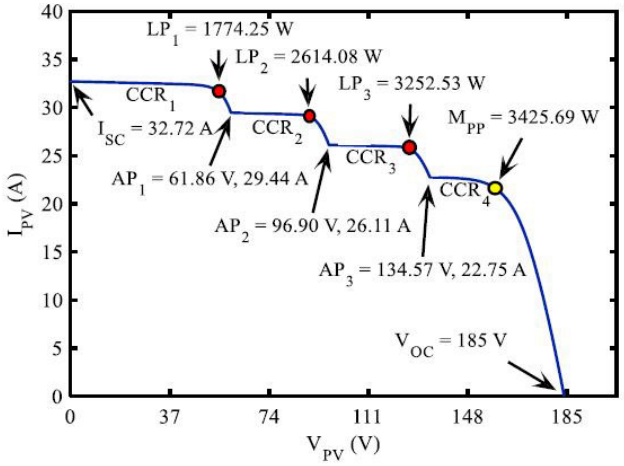

FIGURE 10. IV curve of HC.

A. ANALYSIS ON SERIES CONFIGURATION

Table 5 shows the PV modules PV7, PV8, PV9, PV12, PV13 and PV14 for S configuration are initially deactivated

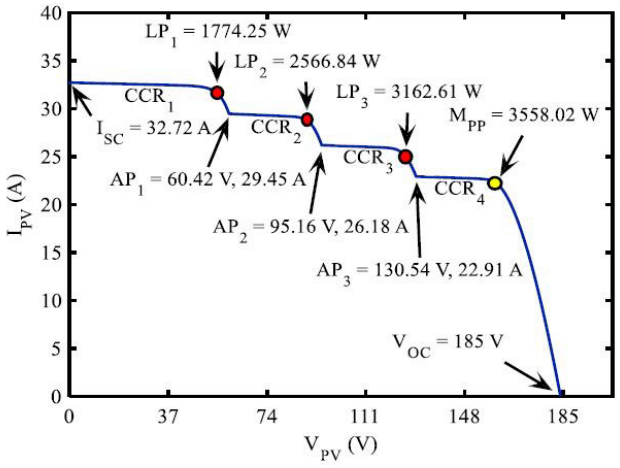

FIGURE 11. IV curve of TCT.

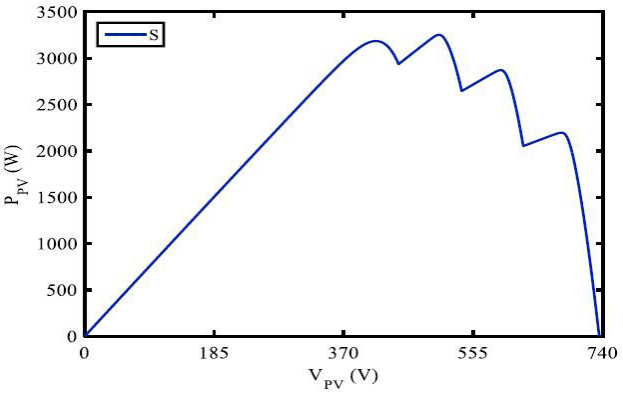

FIGURE 12. PV curve of S configuration.

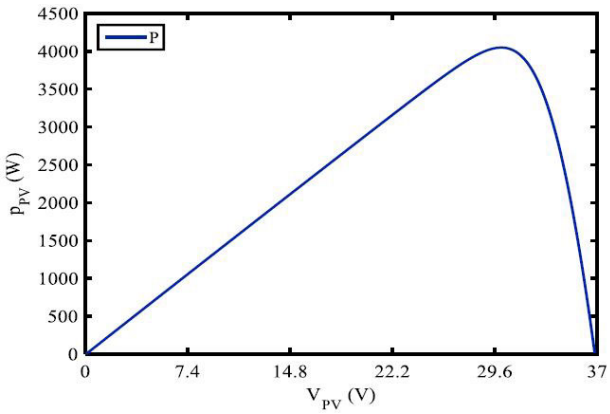

FIGURE 13. PV curve of P configuration.

during constant current region 1 (CCR1) because the modules received low irradiance.

The bypass diodes D7, D8, D9, D12, D13 and D14 are forward biased at this region as shown in Table 6.

CCR1 remained until a point near to 416.95 V, 7.64 A or 3185.5 W which is local point 1 (LP1). Then, PV7 and

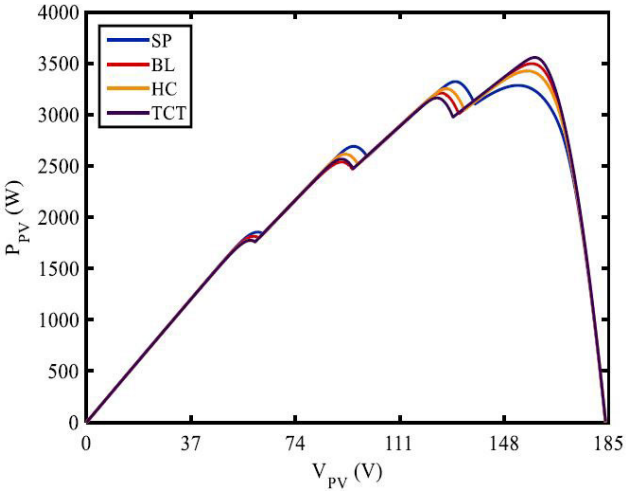

FIGURE 14. PV curve of SP, BL, HC and TCT configurations.

TABLE 4. Shading pattern of PV array.

Configuration	Global Power Peak (P_{MP})
S	3251W
P	4048W
SP	3321W
BL	3496W
HC	3426W
TCT	3558W

PV12 become activated and D7 and D12 become reverse biased at 449.83 V as shown in Fig. 6. This transition creates activation point 1 (AP1). PV8, PV9, PV13, PV14, D8, D9, D13 and D14 remained deactivated and forward biased through CCR2 which constant at 6.55 A. Apart from that, this region shows the maximum point (MP) which is the maximum output power under given shading pattern.

The MP is 3250.77 W which located at 506.35 V as shown in Fig. 12. Consequently, the maximum power point tracker (MPPT) should operate at MP to extract the output power optimally.

Furthermore, the constant current during CCR2 starts to drop at a point near to MP. Next, only PV9 and PV14 remained deactivated and D9 and D14 remained forward biased during CCR3. On the other hand, LP2 occurred at 594.48 V where the current during CCR3 is already dropped at this point. At 627.89 V which is AP3, all bypass diodes in the array are reverse biased because PV9 and PV14 become activated.

B. ANALYSIS ON PARALLEL CONFIGURATION

Fig. 7 shows the single peak IV curve of P configuration due to activation of all PV modules. Even though PV7, PV8,

TABLE 5. The activation or deactivation of PV modules for S configuration (on = activate; off = deactivate) *AP = activation point.

	PV1	PV2	PV3	PV4	PV5	PV6	PV7	PV8	PV9	PV10	PV11	PV12	PV13	PV14	PV15	PV16	PV17	PV18	PV19	PV 20
I_{SC}	on	on	on	on	on	on	off	off	off	on	on	off	off	off	on	on	on	on	on	on
CCR1	on	on	on	on	on	on	off	off	off	on	on	off	off	off	on	on	on	on	on	on
LP1	on	on	on	on	on	on	off	off	off	on	on	off	off	off	on	on	on	on	on	on
AP1	on	on	on	on	on	on	on	off	off	on	on	on	off	off	on	on	on	on	on	on
CCR2	on	on	on	on	on	on	on	off	off	on	on	on	off	off	on	on	on	on	on	on
MP	on	on	on	on	on	on	on	off	off	on	on	on	off	off	on	on	on	on	on	on
AP2	on	on	on	on	on	on	on	on	off	on	on	on	on	off	on	on	on	on	on	on
CCR3	on	on	on	on	on	on	on	on	off	on	on	on	on	off	on	on	on	on	on	on
LP2	on	on	on	on	on	on	on	on	off	on	on	on	on	off	on	on	on	on	on	on
AP3	on	on	on	on	on	on	on	on	on	on	on	on	on	on	on	on	on	on	on	on
CCR4	on	on	on	on	on	on	on	on	on	on	on	on	on	on	on	on	on	on	on	on
LP3	on	on	on	on	on	on	on	on	on	on	on	on	on	on	on	on	on	on	on	on
V_{OC}	on	on	on	on	on	on	on	on	on	on	on	on	on	on	on	on	on	on	on	on

TABLE 6. State of bypass diodes for S configuration (F = forward biased; R = reverse biased) *AP = activation point.

	D1	D2	D3	D4	D5	D6	D7	D8	D9	D10	D11	D12	D13	D14	D15	D16	D17	D18	D19	D 20
I_{SC}	R	R	R	R	R	R	F	F	F	R	R	F	F	F	R	R	R	R	R	R
CCR1	R	R	R	R	R	R	F	F	F	R	R	F	F	F	R	R	R	R	R	R
LP1	R	R	R	R	R	R	F	F	F	R	R	F	F	F	R	R	R	R	R	R
AP1	R	R	R	R	R	R	R	F	F	R	R	R	F	F	R	R	R	R	R	R
CCR2	R	R	R	R	R	R	R	F	F	R	R	R	F	F	R	R	R	R	R	R
MP	R	R	R	R	R	R	R	F	F	R	R	R	F	F	R	R	R	R	R	R
AP2	R	R	R	R	R	R	R	R	F	R	R	R	R	F	R	R	R	R	R	R
CCR3	R	R	R	R	R	R	R	R	F	R	R	R	R	F	R	R	R	R	R	R
LP2	R	R	R	R	R	R	R	R	F	R	R	R	R	F	R	R	R	R	R	R
AP3	R	R	R	R	R	R	R	R	R	R	R	R	R	R	R	R	R	R	R	R
CCR4	R	R	R	R	R	R	R	R	R	R	R	R	R	R	R	R	R	R	R	R
LP3	R	R	R	R	R	R	R	R	R	R	R	R	R	R	R	R	R	R	R	R
V_{OC}	R	R	R	R	R	R	R	R	R	R	R	R	R	R	R	R	R	R	R	R

PV9, PV12, PV13 and PV14 are shaded, all bypass diodes are reverse biased for this configuration. The activation of PV modules and reverse biased bypass diodes will remain through CCR1 which the constant current is 144.12 A. The MP for this configuration is 4048.2 W and located at 30 V. Moreover, no AP occurred in the curve to stop the current drops after CCR1.

C. ANALYSIS ON SERIES PARALLEL CONFIGURATION

For SP configuration, bypass diode D7, D8, D9, D12, D13, and D14, as shown in Table 7 become forward biased during CCR1. This happens because PV modules PV7, PV8, PV9, PV12, PV13 and PV14 deactivated as tabulated in Table 8. The current of CCR1 start to drop near to the 60.61 V, 30.59 A or 1854.06 W which is LP1. The current continues to drop until 29.37 A which is the AP1. AP1 is located at 63.27 V and bypass diode D8, D9, D13, and D14 remained forward biased at this point. This is due to activation of PV modules PV7 and PV12 that are less shaded than PV8, PV9, PV13, and PV14. The states of bypass diodes and PV modules remained unchanged during CCR2.

The current starts to drop near at 94.61 V or 2690.71 W which is LP2. This is continued until AP2 which located at 100.16 V and the states of PV modules and bypass diodes start to change at this point. PV8 and PV13 become activated during CCR3, thus D9 and D12 remains forward biased through this region. The MP for SP configuration on the imposed pattern is 3321.41 W which located at 130.61 V near to CCR3. Thus, MPPT should operate at this point. The current during CCR3 already dropped at this point and continued until AP3 which is 22.53 A. During CCR4, all the bypass diodes are reverse biased due to activation of all PV modules inside SP configuration. The changes from deactivation to activation and forward biased to reverse biased for PV modules and bypass diodes through each region in SP configuration is similar as S configuration.

D. ANALYSIS ON BRIDGE LINK CONFIGURATION

The electrical behaviour of BL is more complicated than S, P, and SP configurations. During CCR1, D3, D4, D7, D8, D9, D12, D13, D14, D18, and D19 become forward biased and their PV modules deactivated respectively at this stage as depicted in Table 9 and Table 10. Even though, PV3, PV4, PV18, and PV19 are fully irradiated but the bypass diode become forward biased because of the current flow through CT1, CT2, CT5, and CT6. However, the current of CCR1 starts to drop at point near LP1 which located at 59.31 V or 1813.7 W. At 61.94 V which is AP1, the PV7 and PV12 activated and their bypass diode turn into reverse biased. The states of bypass diodes and PV modules remained unchanged through CCR2. LP2 is located at 90.24 V, 28.12 A or 2537.55 W. The states of bypass diodes and PV modules start to change at 94.91V which is the AP2. D8 and D13 turn into reverse biased due to activation of PV8 and PV13 at AP2 and remained unchanged through CCR3.

LP3 is at 125.47 V or 3209.52 W and current of CCR3 is already dropped. The remaining deactivated PV modules are activated at 22.79V which is AP3 and it remained activated through CCR4. It also followed by the remaining bypass diodes that turn into reverse biased at this level. In addition, MP is located at 157.69 V. Therefore, MPPT should operate at MP to extract 3495.99 W from BL configuration.

E. ANALYSIS ON HONEYCOMB CONFIGURATION

For HC configuration as depicted in Table 11, PV2, PV3, PV4, PV7, PV8, PV9, PV12, PV13, PV14, PV17, PV18 and PV19 are deactivated during CCR1 due to certain bypass diodes that operate in forward biased. Even though PV7 and PV12 received low irradiance, D7 and D12 are reverse biased as tabulated in Table 12 because current flow through CT1 and CT6. The LP1 is 1774.25W and is occurred at 58.02 V, then, current of CCR1 is dropped. During AP1 located at 61.86V, PV8, PV9, PV12 and PV13 are

TABLE 7. State of bypass diodes for SP configuration (F = forward biased; R = reverse biased) *AP = activation point.

	D1	D2	D3	D4	D5	D6	D7	D8	D9	D10	D11	D12	D13	D14	D15	D16	D17	D18	D19	D 20
I_{SC}	R	R	R	R	R	R	F	F	F	R	R	F	F	F	R	R	R	R	R	R
CCR1	R	R	R	R	R	R	F	F	F	R	R	F	F	F	R	R	R	R	R	R
LP1	R	R	R	R	R	R	F	F	F	R	R	F	F	F	R	R	R	R	R	R
AP1	R	R	R	R	R	R	R	F	F	R	R	R	F	F	R	R	R	R	R	R
CCR2	R	R	R	R	R	R	R	F	F	R	R	R	F	F	R	R	R	R	R	R
LP2	R	R	R	R	R	R	R	F	F	R	R	R	F	F	R	R	R	R	R	R
AP2	R	R	R	R	R	R	R	R	F	R	R	R	R	F	R	R	R	R	R	R
CCR3	R	R	R	R	R	R	R	R	F	R	R	R	R	F	R	R	R	R	R	R
MP	R	R	R	R	R	R	R	R	F	R	R	R	R	F	R	R	R	R	R	R
AP3	R	R	R	R	R	R	R	R	R	R	R	R	R	R	R	R	R	R	R	R
CCR4	R	R	R	R	R	R	R	R	R	R	R	R	R	R	R	R	R	R	R	R
LP3	R	R	R	R	R	R	R	R	R	R	R	R	R	R	R	R	R	R	R	R
V_{OC}	R	R	R	R	R	R	R	R	R	R	R	R	R	R	R	R	R	R	R	R

TABLE 8. The activation or deactivation of PV modules for SP configuration (on = active; off = deactivate) *AP = activation point.

	PV1	PV2	PV3	PV4	PV5	PV6	PV7	PV8	PV9	PV10	PV11	PV12	PV13	PV14	PV15	PV16	PV17	PV18	PV19	PV 20
I_{SC}	on	on	on	on	on	on	off	off	off	on	on	off	off	off	on	on	on	on	on	on
CCR1	on	on	on	on	on	on	off	off	off	on	on	off	off	off	on	on	on	on	on	on
LP1	on	on	on	on	on	on	off	off	off	on	on	off	off	off	on	on	on	on	on	on
AP1	on	on	on	on	on	on	on	off	off	on	on	on	off	off	on	on	on	on	on	on
CCR2	on	on	on	on	on	on	on	off	off	on	on	on	off	off	on	on	on	on	on	on
LP2	on	on	on	on	on	on	on	off	off	on	on	on	off	off	on	on	on	on	on	on
AP2	on	on	on	on	on	on	on	on	off	on	on	on	on	off	on	on	on	on	on	on
CCR3	on	on	on	on	on	on	on	on	off	on	on	on	on	off	on	on	on	on	on	on
MP	on	on	on	on	on	on	on	on	off	on	on	on	on	off	on	on	on	on	on	on
AP3	on	on	on	on	on	on	on	on	on	on	on	on	on	on	on	on	on	on	on	on
CCR4	on	on	on	on	on	on	on	on	on	on	on	on	on	on	on	on	on	on	on	on
LP3	on	on	on	on	on	on	on	on	on	on	on	on	on	on	on	on	on	on	on	on
V_{OC}	on	on	on	on	on	on	on	on	on	on	on	on	on	on	on	on	on	on	on	on

TABLE 9. The activation or deactivation of PV modules for BL configuration (on = activate; off = deactivate) *AP = activation point.

	PV1	PV2	PV3	PV4	PV5	PV6	PV7	PV8	PV9	PV10	PV11	PV12	PV13	PV14	PV15	PV16	PV17	PV18	PV19	PV 20
I_{SC}	on	on	off	off	on	on	off	off	off	on	on	off	off	off	on	on	on	off	off	on
CCR1	on	on	off	off	on	on	off	off	off	on	on	off	off	off	on	on	on	off	off	on
LP1	on	on	off	off	on	on	off	off	off	on	on	off	off	off	on	on	on	off	off	on
AP1	on	on	off	off	on	on	on	off	off	on	on	on	off	off	on	on	on	off	off	on
CCR2	on	on	off	off	on	on	on	off	off	on	on	on	off	off	on	on	on	off	off	on
LP2	on	on	off	off	on	on	on	off	off	on	on	on	off	off	on	on	on	off	off	on
AP2	on	on	off	off	on	on	on	on	off	on	on	on	on	off	on	on	on	off	off	on
CCR3	on	on	off	off	on	on	on	on	off	on	on	on	on	off	on	on	on	off	off	on
MP	on	on	off	off	on	on	on	on	off	on	on	on	on	off	on	on	on	off	off	on
AP3	on	on	on	on	on	on	on	on	on	on	on	on	on	on	on	on	on	on	on	on
CCR4	on	on	on	on	on	on	on	on	on	on	on	on	on	on	on	on	on	on	on	on
LP3	on	on	on	on	on	on	on	on	on	on	on	on	on	on	on	on	on	on	on	on
V_{OC}	on	on	on	on	on	on	on	on	on	on	on	on	on	on	on	on	on	on	on	on

TABLE 10. State of bypass diodes for BL configuration (F = forward biased; R = reverse biased) *AP = activation point.

	PV1	PV2	PV3	PV4	PV5	PV6	PV7	PV8	PV9	PV10	PV11	PV12	PV13	PV14	PV15	PV16	PV17	PV18	PV19	PV 20
I_{SC}	R	R	F	F	R	R	F	F	F	R	R	F	F	F	R	R	R	F	F	R
CCR1	R	R	F	F	R	R	F	F	F	R	R	F	F	F	R	R	R	F	F	R
LP1	R	R	F	F	R	R	F	F	F	R	R	F	F	F	R	R	R	F	F	R
AP1	R	R	F	F	R	R	R	F	F	R	R	R	F	F	R	R	R	F	F	R
CCR2	R	R	F	F	R	R	R	F	F	R	R	R	F	F	R	R	R	F	F	R
LP2	R	R	F	F	R	R	R	F	F	R	R	R	F	F	R	R	R	F	F	R
AP2	R	R	F	F	R	R	R	R	F	R	R	R	R	F	R	R	R	F	F	R
CCR3	R	R	F	F	R	R	R	R	F	R	R	R	R	F	R	R	R	F	F	R
MP	R	R	F	F	R	R	R	R	F	R	R	R	R	F	R	R	R	F	F	R
AP3	R	R	R	R	R	R	R	R	R	R	R	R	R	R	R	R	R	R	R	R
CCR4	R	R	R	R	R	R	R	R	R	R	R	R	R	R	R	R	R	R	R	R
LP3	R	R	R	R	R	R	R	R	R	R	R	R	R	R	R	R	R	R	R	R
V_{OC}	R	R	R	R	R	R	R	R	R	R	R	R	R	R	R	R	R	R	R	R

remained deactivated and D8, D9, D12 and D13 also remained forward biased at this point.

The states of PV modules and bypass diodes remained unchanged through CCR2. Furthermore, LP2 is 2614.08 W and located at 91.69 V. Next, during AP2 that is located at 96.90 V, D8 and D12 turn into reverse biased due to activation of PV8 and PV12. LP3 is 3252.53 W located at 127.5 V which is near to AP3. The remaining PV modules and bypass diodes activated and turn into reverse biased respectively at 134.57 V which is AP3. All PV modules are activated through CCR4 and MP also located near to this region. The MP is 3425.69 W and located at 156.21 V.

F. ANALYSIS ON TOTAL CROSS-TIED CONFIGURATION

The same shading pattern is also implemented on TCT configuration, thus bypass diode on row 2, row 3, and row 4 become forward biased during CCR1 as depicted in Table 14. The PV modules on row 2, row 3, and row 4 are deactivated during CCR1 as shown in Table 13. Besides, in TCT configuration the current is flowing through CT1, CT2, CT3, CT4, CT9, CT10, CT11, and CT12. The current of CCR1 starts to drop near 58.02 V or 1774.25 W which is LP1. During AP1 which located at 60.42 V, the bypass diodes on row 2 switch to reverse biased due to the activation of the PV module on row 2. The states of bypass diodes and PV modules remained unchanged through CCR2. The LP2 is 2566.84 W located at 90.35 V. Then, the bypass diodes on row 4 remained forward biased through CCR3 due to deactivation of PV modules on Row4 that starts from AP2. AP2 and LP3 are located at 95.16 V and 124.17 V respectively. During AP3 which located at 130.54 V, all bypass diodes on TCT configuration switch to reverse biased and all PV modules are activated at this stage. The PV modules and bypass diodes remained activated through CCR4. The point of MP is located near to CCR4 similar with HC and BL configuration. The MP is 3558.02 W located at 158.84 V.

TABLE 11. The activation or deactivation of PV modules for HC configuration (on = activate; off = deactivate) *AP = activation point.

	PV1	PV2	PV3	PV4	PV5	PV6	PV7	PV8	PV9	PV10	PV11	PV12	PV13	PV14	PV15	PV16	PV17	PV18	PV19	PV 20
I_{SC}	on	off	off	off	on	on	off	off	off	on	on	off	off	off	on	on	off	off	off	on
CCR1	on	off	off	off	on	on	off	off	off	on	on	off	off	off	on	on	off	off	off	on
LP1	on	off	off	off	on	on	off	off	off	on	on	off	off	off	on	on	off	off	off	on
AP1	on	on	on	on	on	on	on	off	off	on	on	on	off	off	on	on	on	on	on	on
CCR2	on	on	on	on	on	on	on	off	off	on	on	on	off	off	on	on	on	on	on	on
LP2	on	on	on	on	on	on	on	off	off	on	on	on	off	off	on	on	on	on	on	on
AP2	on	on	on	on	on	on	on	on	off	on	on	on	on	off	on	on	on	on	on	on
CCR3	on	on	on	on	on	on	on	on	off	on	on	on	on	off	on	on	on	on	on	on
MP	on	on	on	on	on	on	on	on	off	on	on	on	on	off	on	on	on	on	on	on
AP3	on	on	on	on	on	on	on	on	on	on	on	on	on	on	on	on	on	on	on	on
CCR4	on	on	on	on	on	on	on	on	on	on	on	on	on	on	on	on	on	on	on	on
LP3	on	on	on	on	on	on	on	on	on	on	on	on	on	on	on	on	on	on	on	on
V_{OC}	on	on	on	on	on	on	on	on	on	on	on	on	on	on	on	on	on	on	on	on

TABLE 12. State of bypass diodes for HC configuration (F = forward biased; R = reverse biased) *AP = activation point.

	PV1	PV2	PV3	PV4	PV5	PV6	PV7	PV8	PV9	PV10	PV11	PV12	PV13	PV14	PV15	PV16	PV17	PV18	PV19	PV 20
I_{SC}	R	F	F	F	R	R	F	F	F	R	R	F	F	F	R	R	F	F	F	R
CCR1	R	F	F	F	R	R	F	F	F	R	R	F	F	F	R	R	F	F	F	R
LP1	R	F	F	F	R	R	F	F	F	R	R	F	F	F	R	R	F	F	F	R
AP1	R	R	R	R	R	R	R	F	F	R	R	R	F	F	R	R	R	R	R	R
CCR2	R	R	R	R	R	R	R	F	F	R	R	R	F	F	R	R	R	R	R	R
LP2	R	R	R	R	R	R	R	F	F	R	R	R	F	F	R	R	R	R	R	R
AP2	R	R	R	R	R	R	R	R	F	R	R	R	R	F	R	R	R	R	R	R
CCR3	R	R	R	R	R	R	R	R	F	R	R	R	R	F	R	R	R	R	R	R
MP	R	R	R	R	R	R	R	R	F	R	R	R	R	F	R	R	R	R	R	R
AP3	R	R	R	R	R	R	R	R	R	R	R	R	R	R	R	R	R	R	R	R
CCR4	R	R	R	R	R	R	R	R	R	R	R	R	R	R	R	R	R	R	R	R
LP3	R	R	R	R	R	R	R	R	R	R	R	R	R	R	R	R	R	R	R	R
V_{OC}	R	R	R	R	R	R	R	R	R	R	R	R	R	R	R	R	R	R	R	R

TABLE 13. The activation or deactivation of PV modules for TCT configuration (on = activate; off = deactivate) *AP = activation point.

	PV1	PV2	PV3	PV4	PV5	PV6	PV7	PV8	PV9	PV10	PV11	PV12	PV13	PV14	PV15	PV16	PV17	PV18	PV19	PV 20
I_{SC}	on	off	off	off	on	on	off	off	off	on	on	off	off	off	on	on	off	off	off	on
CCR1	on	on	off	off	off	on	off	off	off	on	on	off	off	off	on	on	off	off	off	on
LP1	on	on	off	off	off	on	off	off	off	on	on	off	off	off	on	on	off	off	off	on
AP1	on	on	on	off	off	on	on	off	off	on	on	on	off	off	on	on	on	off	off	on
CCR2	on	on	on	off	off	on	on	off	off	on	on	on	off	off	on	on	on	off	off	on
LP2	on	on	on	off	off	on	on	off	off	on	on	on	off	off	on	on	on	off	off	on
AP2	on	on	on	on	off	on	on	on	off	on	on	on	on	off	on	on	on	on	off	on
CCR3	on	on	on	on	off	on	on	on	off	on	on	on	on	off	on	on	on	on	off	on
MP	on	on	on	on	off	on	on	on	off	on	on	on	on	off	on	on	on	on	off	on
AP3	on	on	on	on	on	on	on	on	on	on	on	on	on	on	on	on	on	on	on	on
CCR4	on	on	on	on	on	on	on	on	on	on	on	on	on	on	on	on	on	on	on	on
LP3	on	on	on	on	on	on	on	on	on	on	on	on	on	on	on	on	on	on	on	on
V_{OC}	on	on	on	on	on	on	on	on	on	on	on	on	on	on	on	on	on	on	on	on

G. SUMMARY OF STATIC PV ARRAY RECONFIGURATION PERFORMANCE

As seen in Figs. 8 to 11, the I_{SC} of the PV array ($I_{SC(array)}$) of SP, BL, HC and TCT configurations are the sum of short circuit current through each string ($I_{SC(STR,n)}$) as shown in Eq. 4. The ($I_{SC(STR,n)}$) is the I_{SC} for one PV module in a string because the PV modules are connected in series.

$$I_{sc(array)} = I_{sc(str,1)} + I_{sc(str,2)} + I_{sc(str,3)} + I_{sc(str,4)} \quad (4)$$

For the imposed shading pattern, the I_{SC} of the SP, BL, HC and TCT configurations is 32.72 A. However, for S configuration the $I_{SC}(array)$ is equal as I_{SC} for one PV module which is 8.18 A. Otherwise, the $I_{SC}(array)$ of P configuration is 144.2 A.

Detailed observation on the characteristic of IV curve for both array configurations shows that there is a constant current region (CCRn) between I_{SC} and local point 1 (LP1) then between LP(n) and LP (n + 1). CCR is created due to certain bypass diodes that become forward biased during PSC. The bypass diode becomes forward biased to allow the current from a fully irradiated PV module (1000 W/m^2) to flow across the less irradiated module.

Local point (LPn) and maximum point (MP) occur because a certain bypass diode during CCRn slowly switches to reverse biased. However, if the bypass diode remains forward biased, current of PV array will stay constant at CCRn until it achieves MP. Then, the current of PV array is slightly reduced between LPn and activation point n and between MP and activation point n due to certain bypass diodes that switch slowly to reverse biased at this stage. The last LPn or last MP do not occur due to bypass diode. The cause is that the PV array current should become zero at V_{oc} of PV array. Thus it results in the last LPn or last MP and causes a slight change of PV array current.

PV curves of S, SP, BL, HC and TCT configurations show 4 peaks consisting of local power peak, PLP and global power peak, PMP. Otherwise, P configuration depicted single peak which consisting only PMP. Table 4 shows the highest PMP is produced by P configuration. However, from Fig. 7, the current produced by P configuration is high and it is not suitable for PV system. Thus, the most suitable configuration is TCT with higher output power compared to S, SP, BL and HC configurations.

IV. PERFORMANCE ANALYSES FOR DIFFERENT PARTIAL SHADING PATTERNS

The distribution of shade and the irradiance values on PV array highly affects the maximum power that can be produced by the PV array. The shading strength and pattern are based on the building shape and size, cloud or other materials that block the panels from receiving the sunlight directly.

In this paper, the PV array is shaded by shading patterns that are categorized to 20 patterns of shading shown in Figs. 15-17 for each array size are implemented in this

TABLE 14. State of bypass diodes for TCT configuration (F = forward biased; R = reverse biased) *AP = activation point.

	PV1	PV2	PV3	PV4	PV5	PV6	PV7	PV8	PV9	PV10	PV11	PV12	PV13	PV14	PV15	PV16	PV17	PV18	PV19	PV 20
I_{SC}	R	F	F	F	R	R	F	F	F	R	R	F	F	F	R	R	F	F	F	R
CCR1	R	R	F	F	F	R	F	F	F	R	R	F	F	F	R	R	F	F	F	R
LP1	R	R	F	F	F	R	F	F	F	R	R	F	F	F	R	R	F	F	F	R
AP1	R	R	R	F	F	R	R	F	F	R	R	R	F	F	R	R	R	F	F	R
CCR2	R	R	R	F	F	R	R	F	F	R	R	R	F	F	R	R	R	F	F	R
LP2	R	R	R	F	F	R	R	F	F	R	R	R	F	F	R	R	R	F	F	R
AP2	R	R	R	R	F	R	R	R	F	R	R	R	R	F	R	R	R	R	F	R
CCR3	R	R	R	R	F	R	R	R	F	R	R	R	R	F	R	R	R	R	F	R
MP	R	R	R	R	F	R	R	R	F	R	R	R	R	F	R	R	R	R	F	R
AP3	R	R	R	R	R	R	R	R	R	R	R	R	R	R	R	R	R	R	R	R
CCR4	R	R	R	R	R	R	R	R	R	R	R	R	R	R	R	R	R	R	R	R
LP3	R	R	R	R	R	R	R	R	R	R	R	R	R	R	R	R	R	R	R	R
V_{OC}	R	R	R	R	R	R	R	R	R	R	R	R	R	R	R	R	R	R	R	R

TABLE 15. Simulation results for maximum power under all shading profiles of 4 × 5 array size.

Scenario	Global Maximum Power Peak for each type of Interconnection, W					
	BL	HC	TCT	SP	S	P
Diagonal and Long	2631	2566	2988	2368	2089	3224
Short and Long	2011	2008	2024	1993	1720	2716
Diagonal	3045	3075	3343	2714	2714	3495
Short	2849	2714	2849	2849	2714	3495
Long	3135	3124	3187	3032	2569	3452
Inverse Diagonal and Long	2351	2301	2690	2089	2089	3223
Inverse Short and Long	1969	1814	2017	2040	1520	2622
Inverse Diagonal	3201	3073	3342	2714	2714	3495
Inverse Short	2714	2714	2714	2714	2714	3495
Inverse Long	3137	3170	3262	3035	2468	3545
Downward Ladder	2481	2443	2542	2408	2468	3498
Inverse Downward Ladder	2632	2625	2813	2430	2308	3405
Centre	2051	2036	2087	2038	2233	3132
Double Ladder	2942	2833	3087	2387	2415	3410
L Corner	2264	2216	2292	2198	1773	2897
Column (Left)	2880	2880	2880	2880	1902	2880
Two Corner	2684	2655	3183	2714	2714	3495
Random A	3114	3029	3224	2714	2714	3521
One Corner	2596	2548	2634	2502	2479	3380
Random Two Corner	2617	2394	3144	2714	2714	3401

TABLE 16. Simulation results for maximum power under all shading profiles of 5 × 5 array size.

Scenario	Global Maximum Power Peak for each type of Interconnection, W					
	BL	HC	TCT	SP	S	P
Diagonal and Long	2516	2693	3355	2309	2389	3662
Short and Long	2524	2494	2566	2472	2125	3543
Diagonal	3929	3702	4430	3438	3628	4483
Short	3393	3393	3393	3393	3393	4369
Long	4252	4205	4372	4180	3402	4601
Inverse Diagonal and Long	2921	2914	3182	2904	2678	3941
Inverse Short and Long	2496	2537	2658	2719	2125	3543
Inverse Diagonal	4115	3706	4443	3438	3628	4530
Inverse Short	3393	3393	3393	3393	3393	4369
Inverse Long	4263	4234	4460	4183	3402	4695
Downward Ladder	3599	3581	3631	3429	3402	4648
Inverse Downward Ladder	3780	3732	4033	3433	3393	4555
Centre	3969	3966	4117	3885	3628	4671
Double Ladder	3746	3576	4279	3188	3343	4559
L Corner	3178	3123	3248	3101	2687	3885
Column (Left)	4030	4030	4030	4030	2611	4030
Two Corner	3444	3337	4368	3439	3863	4644
Random A	3643	3562	3741	3438	3628	4669
One Corner	3743	3683	3847	3643	3628	4530
Random Two Corner	3611	3321	4319	3439	3863	4550

TABLE 17. Simulation results for maximum power under all shading profiles of 3 × 10 array size.

Scenario	Global Maximum Power Peak for each type of Interconnection, W					
	BL	HC	TCT	SP	S	P
Diagonal and Long	4295	4490	4891	4100	3838	5250
Short and Long	2344	2344	2348	2343	2222	3538
Diagonal	4127	3953	5243	3774	4072	5243
Long	2485	2485	2485	2485	2485	4142
Short	4605	4550	4804	4550	3542	5179
Inverse Diagonal and Long	4055	3919	4048	3885	3191	4877
Inverse Short and Long	3370	3358	3498	3237	3148	4195
Inverse Diagonal	4137	3978	5243	3774	4072	5243
Inverse Long	2485	2485	2485	2485	2485	4142
Inverse Short	4579	4550	4804	4550	3542	5179
Downward Ladder	5481	5492	5670	5453	4777	5865
Inverse Downward Ladder	5483	5363	5822	5164	4777	5865
Centre	4354	4332	4510	4332	3233	4652
Double Ladder	5070	4979	5702	4978	4274	5708
L Corner	3790	3780	3813	3792	3131	4551
Column (Left)	4835	4836	4836	4836	3133	4836
Two Corner	3739	3771	3932	3710	3131	4692
Random A	3937	4104	5194	4070	3601	5293
One Corner	4183	4181	4253	4181	2660	4370
Random Two Corner	4116	4085	4377	4078	4072	5149

study to emulate PSC occurrences. The PV array size are 5 × 4, 5 × 5 and 3 × 10 had been tested under the various PSC occurrences such in Figs. 15 to 17 to analyse the PV arrays performance, besides, configurations used are S, P, SP, BL, HC and TCT.

This paper will present the results for all of the array sizes. The API156P-230 PV module is utilized for these analyses. The irradiance of the shading is distributed by 4 different irradiance levels which are 1000 W/m^2, 700 W/m^2, 500 W/m^2, and 300 W/m^2 while the ambient temperature is maintained at 25^{0}C. The analyses are carried out based on the percentage of shading strength (SS) and the maximum output power (PMP) for S, P, SP, BL, HC and TCT configurations at different shading patterns. Percentage of SS is the loss of irradiance over the total irradiance without shading of the PV array. The equation of SS is shown in Eq. 5. The shading strength is analyzed through this study to prove the performance of the configurations under different patterns of shading to emulate the PSC.

$$SS(\%) = \frac{Irradiance_{Nonshading} - Irradiance_{shading}}{Irradiance_{Nonshading}} * 100 \tag{5}$$

where $Irradiance_{Nonshading}$ refers to total irradiance of the PV array without shading which is 20 kW/m^2 for 5 × 4 array size, 25 kW/m^2 for 5 × 5 array size and 30 kW/m^2 for 3 × 10 array size. Meanwhile, $Irradiance_{shading}$ is the total irradiance of the PV array under PSC.

The simulation results of the 20 different shading patterns considering the maximum power under all shading profiles of 4 × 5, 5 × 5, 3 × 10, array size is presented in Tables 15, 16, and 17.

Also, the system shading and shading strengths are given in Table. 18.

In addition, the comparison of 5 × 4, 5 × 5, 3 × 10 array size PMP, W along with power loss in % for each shading pattern is visually presented in Figs. 18 to 23. The examples of PV curves for the S, P, BL, HC and TCT under different shading profiles are illustrated in Fig. 24. The bar chart of PMP for the S, P, BL, HC and TCT under different shading profiles are illustrated in Figs. 25 to 42. The results show the relation between maximum output power and the shading

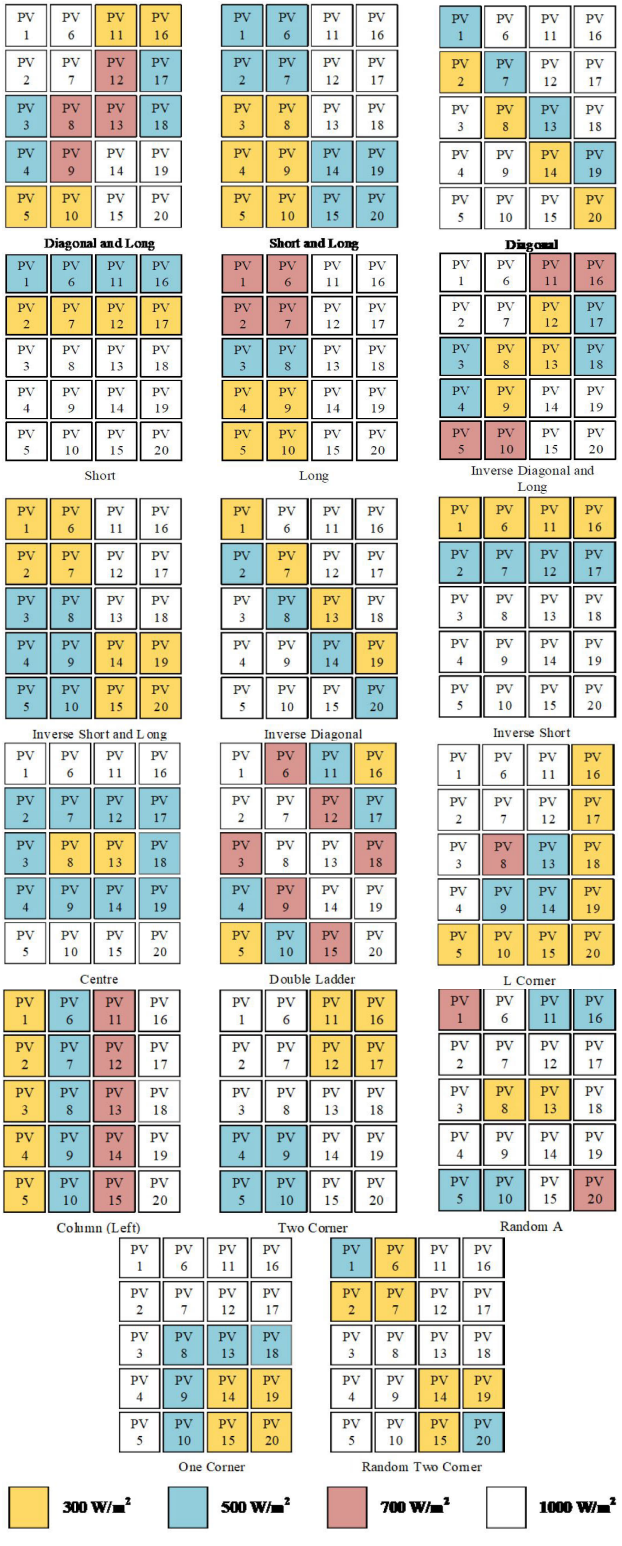

FIGURE 15. Shading patterns of 5 × 4 array size.

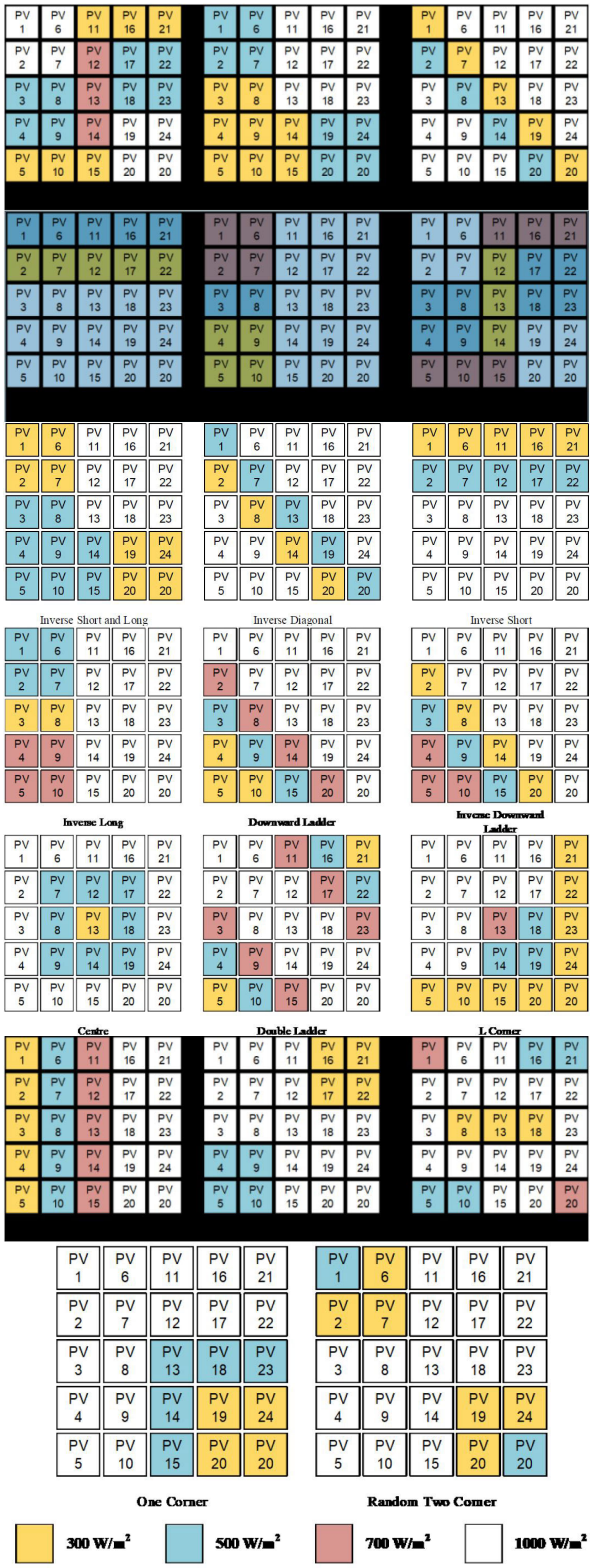

FIGURE 16. Shading patterns of 5 × 5 array size.

pattern where the maximum power depends on the shading pattern of the array.

From the result, Diagonal pattern, Inverse Diagonal pattern, Long pattern, Inverse Long pattern and Random A has the highest output power since all rows of configurations are distributed equally by the shaded modules for 5 × 4 array size. Meanwhile, Diagonal pattern, Inverse Diagonal pattern,

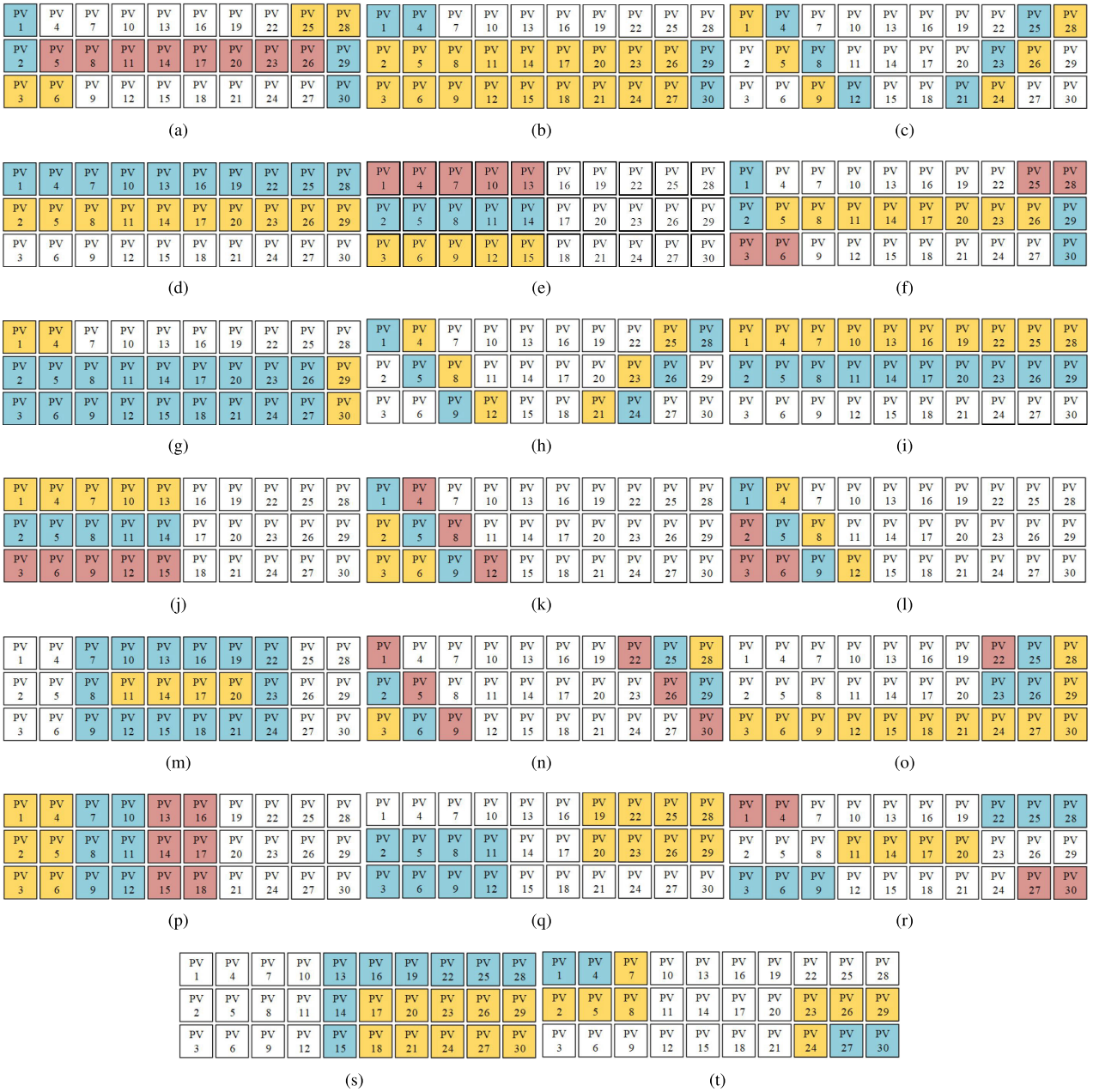

FIGURE 17. Shading patterns of 3 × 10 array size (a) diagonal and long, (b) short and long, (c) diagonal, (d) long (cont.), (e) short, (f) inverse diagonal and long (g) inverse short and long, (h) inverse diagonal, (i) inverse long, (j) inverse short, (k) downward ladder, (l) inverse downward ladder (m) centre, (n) double ladder, (o) L corner, (p) column (left), (q) two corners, (r) random A (s) one corner, (t) random two corners.

Long pattern, Inverse Long pattern and Column Left pattern showed the highest output power among the PSC for 5 × 5 array size.

Furthermore, Downward Ladder pattern, Inverse Downward Ladder pattern, Double Ladder pattern, Column Left pattern, and Short pattern exhibited the highest output power compared to others shading profiles for 3 × 10 array size. If the shade or irradiance values is equally distributed throughout each string such as under Column (Left) condition. Authors found that the PMP produced by P, SP, BL, HC, and TCT schemes under these PSC is equivalent. This condition will cause the IMP is equally produced by each interconnection since there is no limitation of current produced due to the shaded PV panel towards the unshaded PV panels in each string.

However, in case the shade not equally distributed among the rows but throughout the strings, as in Short and Long pattern and Inverse Short and Long pattern, the shading causes more power loss for all of the array size. From the result, the energy yield can be optimized when the shading is distributed equally among rows of the configuration. For all configurations, the complicated shading patterns have the

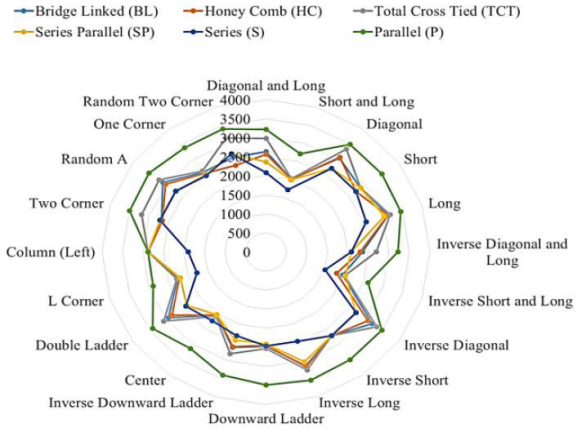

FIGURE 18. Comparison of 5 × 4 array size P_{MP}, W for each shading.

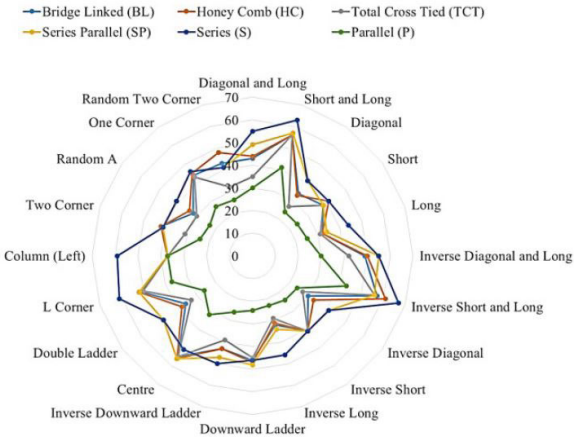

FIGURE 19. Comparison of 5 × 4 array size power losses, % for each shading pattern.

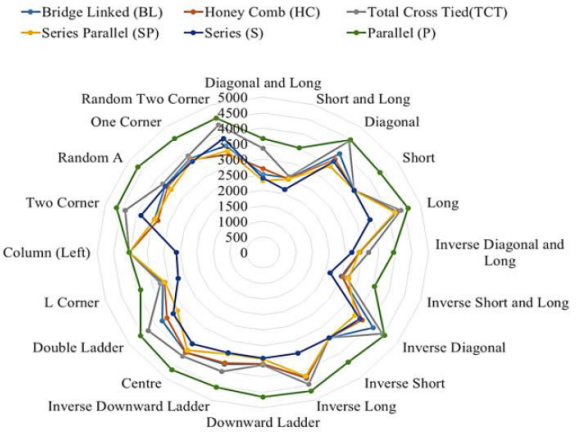

FIGURE 20. Comparison of 5 × 5 array size PMP, W for each shading pattern.

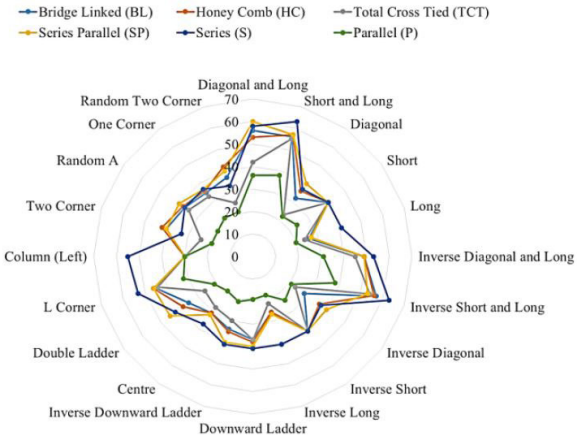

FIGURE 21. Comparison of 5 × 5 array size power losses, % for each shading pattern.

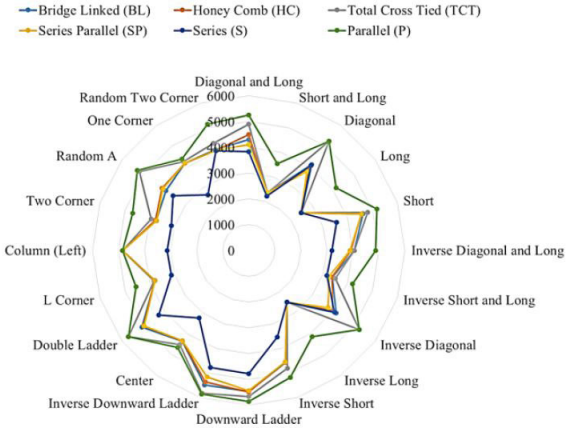

FIGURE 22. Comparison of 3 × 10 array size array size P_{MP}, W for each shading pattern.

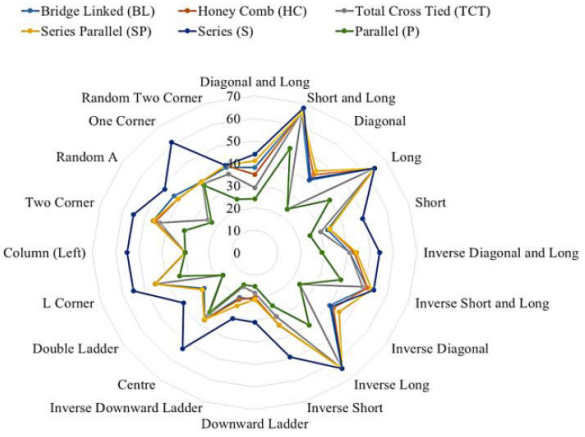

FIGURE 23. Comparison of 3 × 10 array size power losses, % for each shading pattern.

least output power, meanwhile, simple shading patterns, gave the higher energy yield.

From the observations, the TCT configuration is the better choice under any shading pattern since the maximum output power for TCT is higher than S, SP, BL and HC configuration regardless of P configuration in all patterns for all of the array sizes. For Inverse Short pattern, the output power are

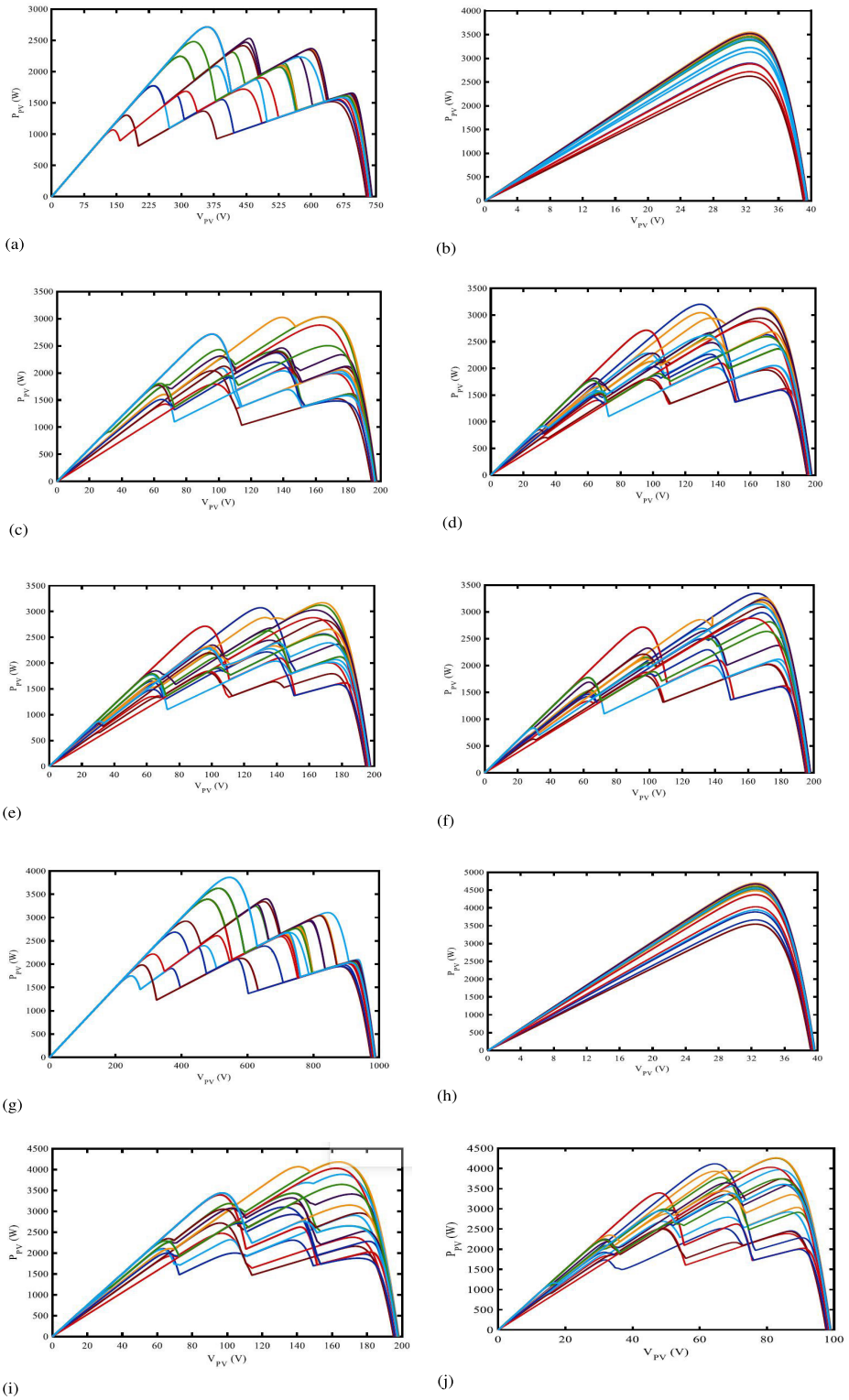

FIGURE 24. Comparison of PV curves under each partial shading pattern (a) for S configuration with 5 × 4 array size, (b) for P configuration with 5 × 4 array size, (c) for SP configuration, (d) for BL configuration with 5 × 4 array size, (e) for HC configuration with 5 × 4 array size, (f) for TCT configuration with 5 × 4 array size, (g) for S configuration with 5 × 5 array size, (h) for P configuration with 5 × 5 array size, (i) for SP configuration with 5 × 5 array size, (j) for BL configuration with 5 × 5 array size, (k) for HC configuration with 5 × 5 array size, (l) for TCT configuration with 5 × 5 array size, (m) for S configuration with 3 × 10 array size, (n) for P configuration with 3 × 10 array size, (o) for SP configuration with 3 × 10 array size, (p) for BL configuration with 3 × 10 array size, (q) for HC configuration with 3 × 10 array size, (r) for TCT configuration with 3 × 10 array size.

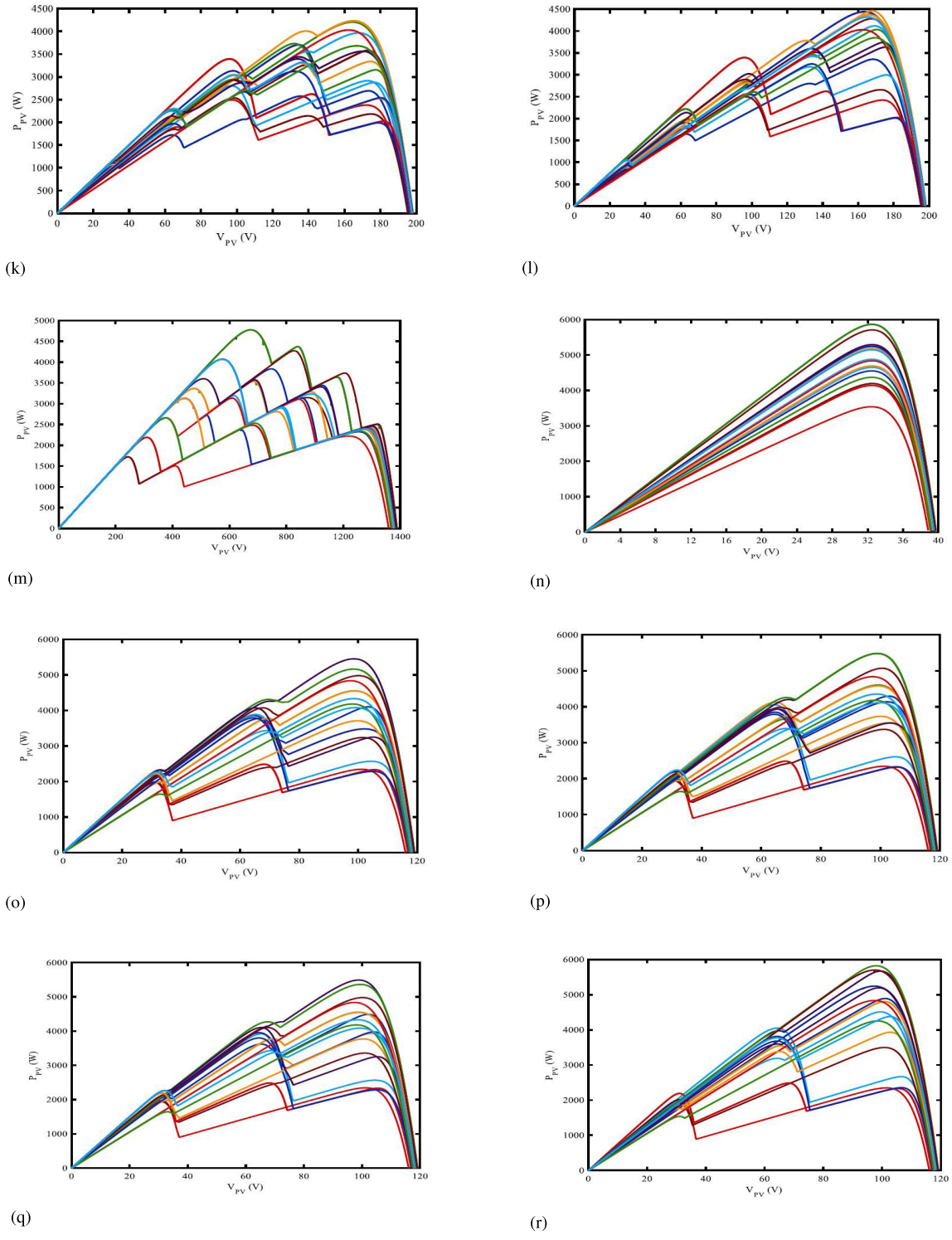

FIGURE 24. *(Continued.)* **Comparison of PV curves under each partial shading pattern (a) for S configuration with 5 × 4 array size, (b) for P configuration with 5 × 4 array size, (c) for SP configuration, (d) for BL configuration with 5 × 4 array size, (e) for HC configuration with 5 × 4 array size, (f) for TCT configuration with 5 × 4 array size, (g) for S configuration with 5 × 5 array size, (h) for P configuration with 5 × 5 array size, (i) for SP configuration with 5 × 5 array size, (j) for BL configuration with 5 × 5 array size, (k) for HC configuration with 5 × 5 array size, (l) for TCT configuration with 5 × 5 array size, (m) for S configuration with 3 × 10 array size, (n) for P configuration with 3 × 10 array size, (o) for SP configuration with 3 × 10 array size, (p) for BL configuration with 3 × 10 array size, (q) for HC configuration with 3 × 10 array size, (r) for TCT configuration with 3 × 10 array size.**

found same for SP, BL, and TCT configurations for 5 × 4 and 5 × 5 PV array sizes. However, this does not dispel the conclusion that the TCT configuration performed better than the other configurations under any given shading pattern.

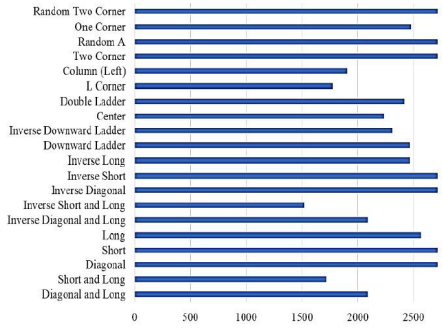

FIGURE 25. Comparison of P_{MP} in Watts for S configuration with 5 × 4 array size under each partial shading pattern.

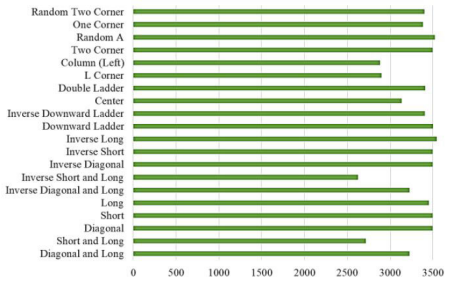

FIGURE 26. Comparison of P_{MP} in Watts for P configuration with 5 × 4 array size under each partial shading pattern.

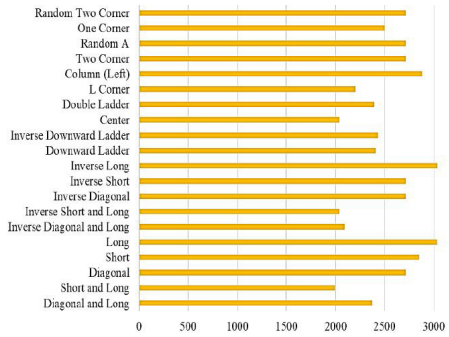

FIGURE 27. Comparison of P_{MP} in Watts for SP configuration with 5 × 4 array size under each partial shading pattern.

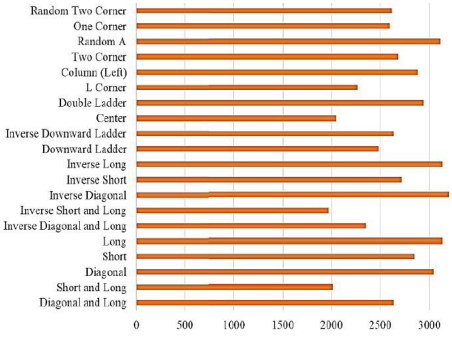

FIGURE 28. Comparison of P_{MP} in Watts for BL configuration with 5 × 4 array size under each partial shading pattern.

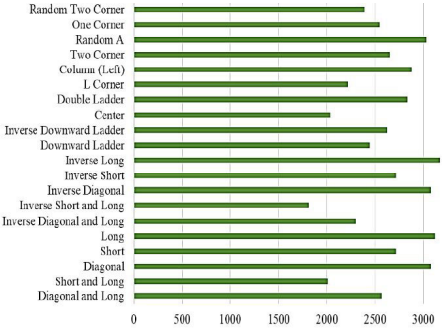

FIGURE 29. Comparison of P_{MP} in Watts for HC configuration with 5 × 4 array size under each partial shading pattern.

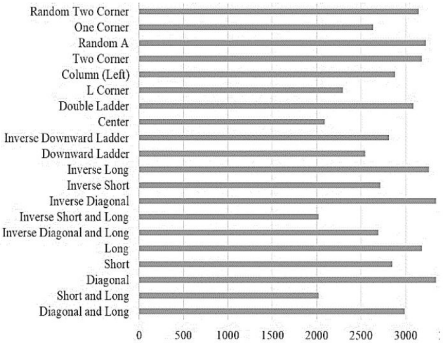

FIGURE 30. Comparison of P_{MP} in Watts for TCT configuration with 5 × 4 array size under each partial shading pattern.

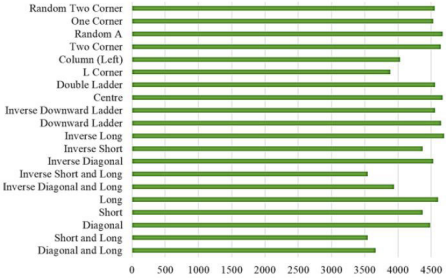

FIGURE 31. Comparison of P_{MP} in Watts for S configuration with 5 × 5 array size under each partial shading pattern.

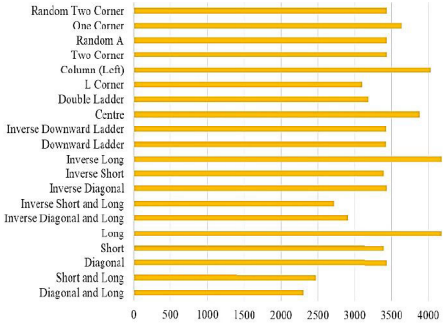

FIGURE 32. Comparison of P_{MP} in Watts for P configuration with 5 × 5 array size under each partial shading pattern.

However, it is found that one shading pattern which is SP configuration significantly outperform the TCT configuration by giving higher PMP for 5 × 4 array size and 5 × 5 array size. The PSC mentioned by the authors is Inverse and Short pattern whereas the SS was 43% for whereas the highest percentage of SS compared to other PSC for 5 × 4 array size, besides, 38% which also the highest SS percentage

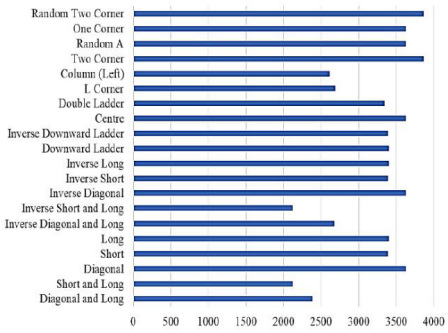

FIGURE 33. Comparison of P_{MP} in Watts for SP configuration with 5 × 5 array size under each partial shading pattern.

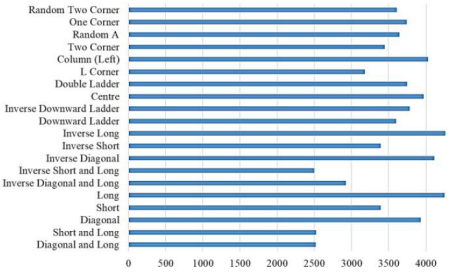

FIGURE 34. Comparison of P_{MP} in Watts for BL configuration with 5 × 5 array size under each partial shading pattern.

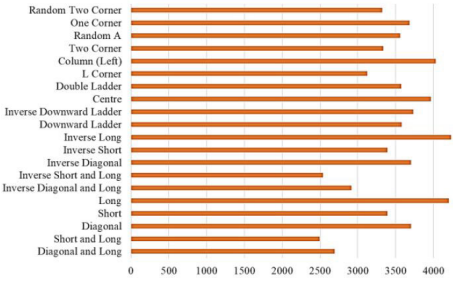

FIGURE 35. Comparison of P_{MP} in Watts for HC configuration with 5 × 5 array size under each partial shading pattern.

for 5 × 5 array size and Figure 43 illustrated the shading pattern, besides, current produced by each string for both configurations.

From the Fig. 43, it can be clearly seen that the current produced for each string by the SP configuration for both array sizes is higher compare to TCT configuration, even though, the voltage generated by TCT configuration is higher. This shading condition created a gap of current produced by each string for both configurations of 5 × 4 array size which is about 2.7 A for $I_{String1}$ and $I_{String2}$ whereas 2.4 A for $I_{String3}$ and $I_{String4}$, meanwhile, the current gap created for both configurations with 5 × 5 array size are 2.9 A for $I_{String1}$ and $I_{String2}$, 2.8 A for $I_{String3}$ and 2.7 A for $I_{String4}$ and $I_{String5}$. Therefore, resulting a lower IMP for TCT configuration approximately half of value compared to SP configuration

As the percentage of SS increase, the PV arrays' mismatch losses increase, and efficiency drop.

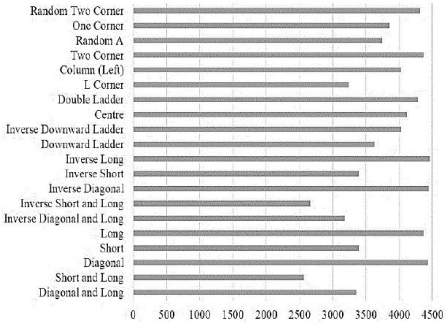

FIGURE 36. Comparison of P_{MP} in Watts for TCT configuration with 5 × 5 array size under each partial shading pattern.

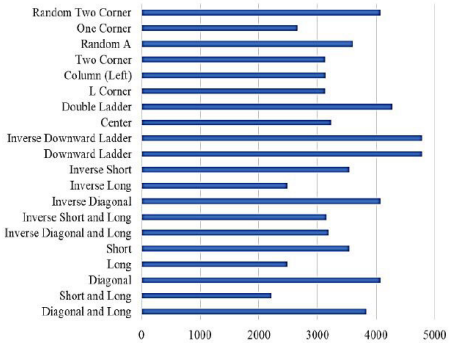

FIGURE 37. Comparison of P_{MP} in Watts for S configuration with 3 × 10 array size under each partial shading pattern.

FIGURE 38. Comparison of P_{MP} in Watts for P configuration with 3 × 10 array size under each partial shading pattern.

Thus, it is important noticing that, under a certain PSC for a PV array with N panels, the PMP extraction from the PV array is either approximately equal or lower than the sum of PMP that delivered by each panel which become a root to BDs activation due to the constraints occurred which make the corresponding PV arrays become short circuited and reduce the PMP at the PV array terminals. Therefore, the PMP produced under PSCs does not equivalent as the PMP available in the panels.

In addition, as discussed before based on Kirchhoff's Current Law, the limitation of current produced in each series string caused by the shaded PV modules towards unshaded

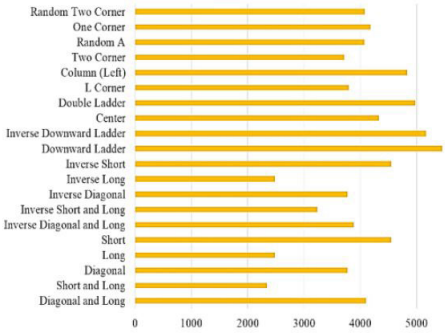

FIGURE 39. Comparison of P_{MP} in Watts for SP configuration with 3 × 10 array size under each partial shading pattern.

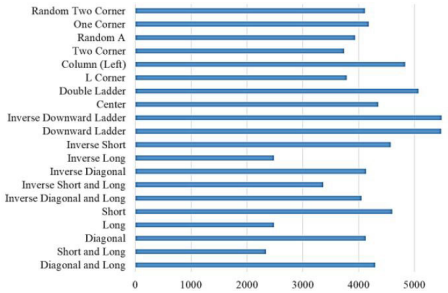

FIGURE 40. Comparison of P_{MP} in Watts for B; configuration with 3 × 10 array size under each partial shading pattern.

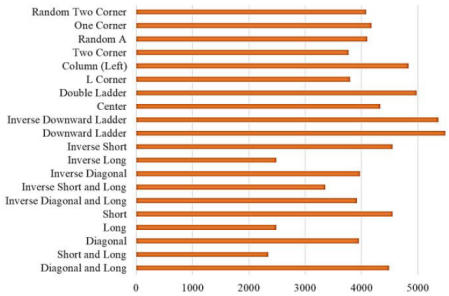

FIGURE 41. Comparison of P_{MP} in Watts for HC configuration with 3 × 10 array size under each partial shading pattern.

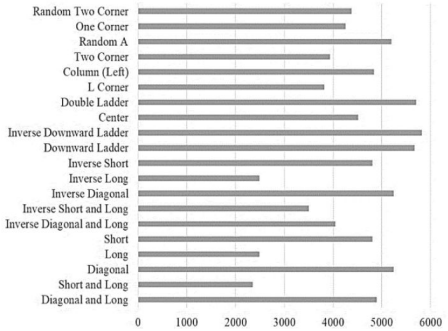

FIGURE 42. Comparison of P_{MP} in Watts for TCT configuration with 3 × 10 array size under each partial shading pattern.

PV modules will trigger AP at certain value of voltage due to the lower current produced by the shaded PV modules between CCR of the shaded PV modules and unshaded PV modules in the IV curve.

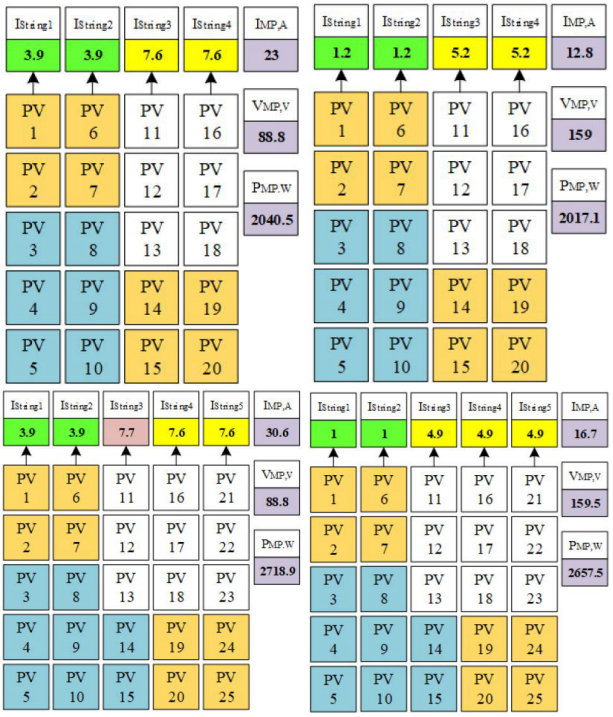

FIGURE 43. The simulation results of 5 × 4 and 5 × 5 array size for $I_{string1}$, $I_{string2}$, $I_{string3}$, $I_{string4}$, I_{MP}, V_{MP}, and P_{MP} under inverse short and long scenario.

TABLE 18. System shading and shading strength of each shading pattern.

Shading Pattern	Shading Strength (%)		
	5×4	5×5	3×10
Diagonal and Long	30	36	24
Short and Long	41	38	67
Diagonal	24	22	24
Short	24	24	25
Long	25	20	40
Inverse Diagonal and Long	30	32	37
Inverse Short and Long	43	38	39
Inverse Diagonal	24	21	24
Inverse Short	24	24	25
Inverse Long	23	18	40
Downward Ladder	24	19	15
Inverse Downward Ladder	26	21	15
Centre	32	19	33
Double Ladder	26	21	17
L Corner	37	32	34
Column (Left)	38	30	30
Two Corner	24	19	32
Random A	20	19	23
One Corner	27	21	37
Random Two Corner	26	21	25

The bypass diode of shaded PV modules will become forward biased due to the excessive current flow produced by the unshaded PV modules.

The SS affects the performance of the PV array configurations in this study and based on the simulation test done, this shows that the concentration or the SS is related to the output power of the array configurations.

Observation made for the result of different shading patterns using S, P, SP, BL, HC and TCT configurations as follows:

1) The maximum output power increase when shade distributed equally among the strings of the configurations.
2) TCT configuration produce higher output power compared to other configurations under most PSC.

V. CONCLUSION

This study presents the detailed analysis of S, P, SP, BL, HC and TCT configurations when subjected to multiple shading patterns. The contribution that stands out in this work is the detail expression of the bypass diode behaviours, which may help many new researchers to comprehend PV configuration techniques easily. Besides, this investigation was performed on three different size PV arrays which makes the outcome more conclusive and reliable. In total twenty shading patterns were tested. The overall results show that the TCT configuration offers better performance compared to the other configurations. In TCT, the parallel links among strings in TCT configuration are more effective for the current flow through the configuration during mismatch or PSCs However, TCT cannot be the optimum candidate for every shading pattern. It is clear from the several shading patterns that on multiple occasions BL and HC outperforms TCT. In some cases, even SP is the best candidate to mitigate partial shading effect. Thus, if the PV engineers/designers has prior knowledge on the expected shading in an area, they can choose the suitable PV configuration for that particular place.

In addition, this study also shows that the pattern of shading is also one of the eminent factors that affect the energy yields of a PV array. If more shades distributed among the Strings, the power loss is increased. On the other hand, distributing the shading among the Rows of the configuration optimizes the energy yield of the PV array. Based on such observation, PV array reconfiguration techniques can be a good solution where module connections are re arranged according to the shadow positions. It is envisaged that, this work will help many new researchers to comprehend PV array configuration techniques and produce better solution in the near future.

ACKNOWLEDGMENT

The authors would like to thank the Universiti Malaysia Perlis and the Ministry of Education (MOE) Malaysia for providing the facilities.

REFERENCES

[1] Z. M. Salameh and F. Dagher, "The effect of electrical array reconfiguration on the performance of a PV-powered volumetric water pump," *IEEE Trans. Energy Convers.*, vol. 5, no. 4, pp. 653–658, Dec. 1990.
[2] N. D. Kaushika and N. K. Gautam, "Energy yield simulations of interconnected solar PV arrays," *IEEE Trans. Energy Convers.*, vol. 18, no. 1, pp. 127–134, Mar. 2003.
[3] M. F. N. Tajuddin, M. S. Arif, S. M. Ayob, and Z. Salam, "Perturbative methods for maximum power point tracking (MPPT) of photovoltaic (PV) systems: A review," *Int. J. Energy Res.*, vol. 39, no. 9, pp. 1153–1178, Jul. 2015.
[4] B. Liu and S. Duan, "Energy efficiency evaluation of building integrated photovoltaic systems with different power configurations," *Simul. Model. Pract. Theory*, vol. 29, pp. 93–108, Dec. 2012. [Online]. Available: https://www.sciencedirect.com/science/article/pii/S1569190X12001220
[5] N. M. Kumar, K. Sudhakar, and M. Samykano, "Performance of thin-film BIPV as double sloped pitched roof in buildings of Malaysia," *Energy Sour., A, Recovery, Utilization, Environ. Effects*, vol. 40, no. 20, pp. 2476–2484, Oct. 2018.
[6] N. M. Kumar, K. Sudhakar, and M. Samykano, "Performance comparison of BAPV and BIPV systems with c-Si, CIS and CdTe photovoltaic technologies under tropical weather conditions," *Case Stud. Thermal Eng.*, vol. 13, Mar. 2019, Art. no. 100374. [Online]. Available: https://www.sciencedirect.com/science/article/pii/S2214157X18303940
[7] A. M. Ajmal, T. Sudhakar Babu, V. K. Ramachandaramurthy, D. Yousri, and J. B. Ekanayake, "Static and dynamic reconfiguration approaches for mitigation of partial shading influence in photovoltaic arrays," *Sustain. Energy Technol. Assessments*, vol. 40, Aug. 2020, Art. no. 100738. [Online]. Available: https://www.sciencedirect.com/science/article/pii/S2213138819309361
[8] N. van der Borg and M. Jansen, "Energy loss due to shading in a bipv application," in *Proc. 3rd World Conf. Photovoltaic Energy Convers.*, vol. 3, 2003, pp. 2220–2222.
[9] K. Ş. Parlak, "PV array reconfiguration method under partial shading conditions," *Int. J. Electr. Power Energy Syst.*, vol. 63, pp. 713–721, Dec. 2014. [Online]. Available: https://www.sciencedirect.com/science/article/pii/S0142061514003913
[10] V. Quaschning and R. Hanitsch, "Numerical simulation of current-voltage characteristics of photovoltaic systems with shaded solar cells," *Sol. Energy*, vol. 56, no. 6, pp. 513–520, Jun. 1996.
[11] L. F. L. Villa, D. Picault, B. Raison, S. Bacha, and A. Labonne, "Maximizing the power output of partially shaded photovoltaic plants through optimization of the interconnections among its modules," *IEEE J. Photovolt.*, vol. 2, no. 2, pp. 154–163, Apr. 2012.
[12] A. Bidram, A. Davoudi, and R. S. Balog, "Control and circuit techniques to mitigate partial shading effects in photovoltaic arrays," *IEEE J. Photovolt.*, vol. 2, no. 4, pp. 532–546, Oct. 2012.
[13] M. Miyatake, M. Veerachary, F. Toriumi, N. Fujii, and H. Ko, "Maximum power point tracking of multiple photovoltaic arrays: A PSO approach," *IEEE Trans. Aerosp. Electron. Syst.*, vol. 47, no. 1, pp. 367–380, Jan. 2011.
[14] A. Murtaza, M. Chiaberge, F. Spertino, D. Boero, and M. De Giuseppe, "A maximum power point tracking technique based on bypass diode mechanism for PV arrays under partial shading," *Energy Buildings*, vol. 73, pp. 13–25, Apr. 2014.
[15] I. Houssamo, F. Locment, and M. Sechilariu, "Maximum power tracking for photovoltaic power system: Development and experimental comparison of two algorithms," *Renew. Energy*, vol. 35, no. 10, pp. 2381–2387, Oct. 2010. [Online]. Available: https://www.sciencedirect.com/science/article/pii/S0960148110001588
[16] M. F. N. Tajuddin, S. M. Ayob, Z. Salam, and M. S. Saad, "Evolutionary based maximum power point tracking technique using differential evolution algorithm," *Energy Buildings*, vol. 67, pp. 245–252, Dec. 2013.
[17] F. Belhachat and C. Larbes, "Modeling, analysis and comparison of solar photovoltaic array configurations under partial shading conditions," *Sol. Energy*, vol. 120, pp. 399–418, Oct. 2015.
[18] M. F. N. Tajuddin, S. M. Ayob, and Z. Salam, "Tracking of maximum power point in partial shading condition using differential evolution (DE)," in *Proc. IEEE Int. Conf. Power Energy (PECon)*, Dec. 2012, pp. 384–389.
[19] R. Ramaprabha and B. L. Mathur, "A comprehensive review and analysis of solar photovoltaic array configurations under partial shaded conditions," *Int. J. Photoenergy*, vol. 2012, Mar. 2012, Art. no. 120214.
[20] M. Premkumar, U. Subramaniam, T. S. Babu, R. M. Elavarasan, and L. Mihet-Popa, "Evaluation of mathematical model to characterize the performance of conventional and hybrid PV array topologies under static and dynamic shading patterns," *Energies*, vol. 13, no. 12, p. 3216, Jun. 2020.
[21] Y.-J. Wang and P.-C. Hsu, "An investigation on partial shading of PV modules with different connection configurations of PV cells," *Energy*, vol. 36, no. 5, pp. 3069–3078, May 2011. [Online]. Available: https://www.sciencedirect.com/science/article/pii/S0360544211001484
[22] P. Srinivasa Rao, P. Dinesh, G. Saravana Ilango, and C. Nagamani, "Optimal Su-Do-Ku based interconnection scheme for increased power output from PV array under partial shading conditions," *Frontiers Energy*, vol. 9, no. 2, pp. 199–210, Jun. 2015.

[23] S. Vijayalekshmy, G. R. Bindu, and S. R. Iyer, "Performance comparison of Zig-Zag and Su do Ku schemes in a partially shaded photo voltaic array under static shadow conditions," in *Proc. Innov. Power Adv. Comput. Technol.*, Apr. 2017, pp. 1–6.
[24] T. S. Babu, D. Yousri, and K. Balasubramanian, "Photovoltaic array reconfiguration system for maximizing the harvested power using population-based algorithms," *IEEE Access*, vol. 8, pp. 109608–109624, 2020.
[25] D. Yousri, T. S. Babu, S. Mirjalili, N. Rajasekar, and M. A. Elaziz, "A novel objective function with artificial ecosystem-based optimization for relieving the mismatching power loss of large-scale photovoltaic array," *Energy Convers. Manage.*, vol. 225, Dec. 2020, Art. no. 113385.
[26] D. Yousri, S. B. Thanikanti, K. Balasubramanian, A. Osama, and A. Fathy, "Multi-objective grey wolf optimizer for optimal design of switching matrix for shaded PV array dynamic reconfiguration," *IEEE Access*, vol. 8, pp. 159931–159946, 2020.
[27] B. I. Rani, G. S. Ilango, and C. Nagamani, "Enhanced power generation from PV array under partial shading conditions by shade dispersion using Su Do Ku configuration," *IEEE Trans. Sustain. Energy*, vol. 4, no. 3, pp. 594–601, Jul. 2013.
[28] D. Yousri, T. S. Babu, E. Beshr, M. B. Eteiba, and D. Allam, "A robust strategy based on marine predators algorithm for large scale photovoltaic array reconfiguration to mitigate the partial shading effect on the performance of PV system," *IEEE Access*, vol. 8, pp. 112407–112426, 2020.
[29] R. K. Pachauri, J. Bai, I. Kansal, O. P. Mahela, and B. Khan, "Shade dispersion methodologies for performance improvement of classical total cross-tied photovoltaic array configuration under partial shading conditions," *IET Renew. Power Gener.*, vol. 15, no. 8, pp. 1796–1811, Jun. 2021.
[30] O. Bingöl and B. Özkaya, "Analysis and comparison of different PV array configurations under partial shading conditions," *Sol. Energy*, vol. 160, pp. 336–343, Jan. 2018.
[31] M. Dhimish, V. Holmes, B. Mehrdadi, M. Dales, B. Chong, and L. Zhang, "Seven indicators variations for multiple PV array configurations under partial shading and faulty PV conditions," *Renew. Energy*, vol. 113, pp. 438–460, Dec. 2017.
[32] J. W. Bishop, "Computer simulation of the effects of electrical mismatches in photovoltaic cell interconnection circuits," *Sol. Cells*, vol. 25, no. 1, pp. 73–89, Oct. 1988. [Online]. Available: https://www.sciencedirect.com/science/article/pii/0379678788900592
[33] M. A. Shamshuddin, S. B. Thanikanti, T. Dragicevic, M. Miyatake, and R. Natarajan, "Priority-based energy management technique for integration of solar PV, battery, and fuel cell systems in an autonomous DC microgrid," *Electr. Power Compon. Syst.*, vol. 45, pp. 1–11, Jan. 2018.
[34] N. Belhaouas, M.-S.-A. Cheikh, P. Agathoklis, M.-R. Oularbi, B. Amrouche, K. Sedraoui, and N. Djilali, "PV array power output maximization under partial shading using new shifted PV array arrangements," *Appl. Energy*, vol. 187, pp. 326–337, Feb. 2017.
[35] J. Ahmed and Z. Salam, "An improved method to predict the position of maximum power point during partial shading for PV arrays," *IEEE Trans. Ind. Informat.*, vol. 11, no. 6, pp. 1378–1387, Dec. 2015.
[36] K. Ishaque, Z. Salam, and S. Syafaruddin, "A comprehensive MATLAB Simulink PV system simulator with partial shading capability based on two-diode model," *Solar Energy*, vol. 85, pp. 2217–2227, Sep. 2011. [Online]. Available: https://www.sciencedirect.com/science/article/pii/S0038092X11002118
[37] S. Malathy and R. Ramaprabha, "Comprehensive analysis on the role of array size and configuration on energy yield of photovoltaic systems under shaded conditions," *Renew. Sustain. Energy Rev.*, vol. 49, pp. 672–679, Sep. 2015.

MOHAMMAD NOR RAFIQ NAZER received the B.Eng. degree in electrical engineering from the Universiti Malaysia Perlis (UniMAP), Malaysia, in 2016, where he is currently pursuing the M.Sc. degree in electrical engineering with the Faculty of Electrical Engineering Technology. His research interests include power electronics, photovoltaic systems, PV array reconfiguration techniques, and optimization algorithms.

ABDULFATTAH NOORWALI (Member, IEEE) received the Ph.D. degree in electrical and computer engineering from the University of Western Ontario, London, ON, Canada, in 2017. The title of his thesis was Modeling and Analysis of Smart Grids for Critical Data Communication. He is currently the Chairman of the Electrical and Computer Engineering Department, Faculty of Engineering and Islamic Architecture, Umm Al-Qura University, where he is also an Assistance Professor. He is also a Senior Consultant with Umm Al-Qura Consultancy Oasis, Institute of Consulting Research and Studies (ICRS), Umm Al-Qura University, where he is also the Chairman of Vision Office of Consultancy. He has authored many technical articles in journals and international conferences. His research interests include smart grid communications, cooperative communications, wireless networks, the Internet of Things, crowd management applications, and smart city solutions.

MOHAMMAD FARIDUN NAIM TAJUDDIN received the B.Eng. and M.Eng. degrees from the University of Malaya (UM), Malaysia, in 2004 and 2007, respectively, and the Ph.D. degree from the Universiti Teknologi Malaysia (UTM), Johor, Malaysia, in 2015. He is currently with the Faculty of Electrical Engineering Technology, Universiti Malaysia Perlis (UniMAP). He has published refereed manuscripts in various reputable international journals. His research interests include power electronics control, photovoltaic modeling and control, intelligent control, and optimization techniques. He is also acting as a Reviewer of various reputed journals, such as the IEEE, Elsevier *Applied Energy*, *Renewable and Sustainable Energy Reviews*, *Neurocomputing*, and *Energy Reports*.

MOHAMMAD ZUBAIR KHAN received the Ph.D. degree in computer science and information technology from the Faculty of Engineering, M. J. P. Rohilkhand University, Bareilly, India, and the Master of Technology degree in computer science and engineering from U. P. Technical University, Lucknow, India. He worked as the Head and an Associate Professor with the Department of Computer Science and Engineering, Invertis University, Bareilly. He is currently working as an Associate Professor with the Department of Computer Science, College of Computer Science and Engineering, Taibah University. He has published more than 60 journal articles and conference papers. His research interests include the IoT, machine learning, parallel and distributed computing, and computer networks. He has more than 15 years teaching and research experience. Since 2004, he has been a member of the Computer Society of India.

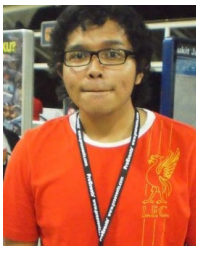

MOHAMAD AFIQ IZZAT AHMAD TAZALLY received the B.Eng. degree in electrical engineering from the Universiti Malaysia Perlis (UniMAP), Malaysia, in 2015, where he is currently pursuing the M.Sc. degree in electrical engineering with the Faculty of Electrical Engineering Technology. His research interests include power electronics, photovoltaic systems, PV array reconfiguration techniques, and optimization algorithms.

JUBAER AHMED (Member, IEEE) received the B.Sc. degree in electrical and electronics engineering from Bangladesh University of Engineering and Technology, Dhaka, Bangladesh, in 2012, and the Ph.D. degree in electrical engineering from the Universiti Teknologi Malaysia, Johor Bahru, Malaysia, in 2016. He is currently a Lecturer with the Swinburne University of Technology Sarawak, Kuching, Malaysia. His research interests include photovoltaic modeling and control, energy conversion from renewable sources, and power electronics.

THANIKANTI SUDHAKAR BABU (Senior Member, IEEE) received the B.Tech. degree from Jawaharlal Nehru Technological University at Ananthapur, Ananthapur, India, in 2009, the M.Tech. degree in power electronics and industrial drives from Anna University, Chennai, India, in 2011, and the Ph.D. degree from VIT University, Vellore, India, in 2017.

From 2019 to 2020, he was associated as a Postdoctoral Researcher with the Institute of Power Engineering, Universiti Tenaga Nasional (UNITEN), Malaysia. He is currently working as an Associate Professor with the Department of Electrical Engineering, Chaitanya Bharathi Institute of Technology, Hyderabad, India. He has published more than 85 research articles in various renowned international journals, including over 55 in SCI-indexed journals, and more than 15 papers in international conferences. His research interests include the design and implementation of solar PV systems, renewable energy resources, power management for hybrid energy systems, storage systems, fuel cell technologies, electric vehicles, and smart grids. He has been acting as an Editorial Board Member and a Reviewer of various reputed journals, such as the IEEE and IEEE Access, IET, Elsevier, and Taylor & Francis.

NUR HAFIZAH GHAZALI (Member, IEEE) received the B.Sc. degree from the Universiti Teknologi Malaysia (UTM), Johor, Malaysia, in 2006, the M.Sc. degree from the Universiti Utara Malaysia (UUM), Malaysia, in 2010, and the Ph.D. degree from UTM, in 2015. She is currently with the Faculty of Electronic Engineering, Universiti Malaysia Perlis (UniMAP). Her research interests include artificial intelligence, optimization algorithms, image processing, and data hiding.

CHINMAY CHAKRABORTY received the B.Tech. degree in electronics and communication engineering from MAKAUT, India, in 2006, the M.S. degree in telecommunication engineering from IIT Kharagpur, Kharagpur, India, in 2010, and the Ph.D. degree in electronics and communication engineering from the Birla Institute of Technology, Mesra, India. He is currently an Assistant Professor with the Department of Electronics and Communication Engineering, BIT Mesra. Before BIT, he worked as a Research Consultant with the Coal India project at Industrial Engineering and Management, IIT Kharagpur. He worked as a Project Coordinator of Telecom Convergence Switch project under the Indo-U.S. joint initiative. He also worked as a Network Engineer in System Administration at MISPL under Global Teleservices Ltd., India. He has authored the book *PSTN-IP Telephony Gateway for Ensuring QoS in Heterogeneous Networks*, *Advanced Classification Techniques for Healthcare Analysis*, and *Smart Medical Data Sensing and IoT Systems Design in Healthcare*. His research interests include wireless body area networks, the Internet of Medical Things, energy-efficient wireless communications and networking, and point-of-care diagnosis. He received the Young Research Excellence Award, the Global Peer Review Award, the Young Faculty Award, and the Outstanding Researcher Award.

NALLAPANENI MANOJ KUMAR (Member, IEEE) received the B.Tech. degree in electrical and electronics engineering from GITAM University, Visakhapatnam, India, the M.Tech. degree in renewable energy technologies from Karunya University, Coimbatore, India, the M.A. degree in environmental economics from Annamalai University (Directorate of Distance Education), Chidambaram, India, and the Ph.D. degree in blockchain for circular economy from the City University of Hong Kong, Hong Kong.

He worked as an Assistant Professor with the Department of Electrical and Electronics Engineering, Bharat Institute of Engineering and Technology, Hyderabad, India, and an Energy Engineer at Atiode Solar Systems Ltd., Nigeria. He was a Research Fellow with the University of Malaysia Pahang worked on the project "Solar Photovoltaics as Urban Infrastructure." He is currently working as a Postdoctoral Research Fellow with the School of Energy and Environment, City University of Hong Kong. He has published 14 chapters in scientific books, more than 115 research articles in scientific journals, including over 60 in SCI-indexed journals, and more than 38 papers in international conferences. His research interests broadly fall under sustainable and resilient infrastructure creation in the related fields of energy and the environment. His research interests include renewable energy, building integrated photovoltaic systems, energy management, modeling and performance investigation of energy systems, building energy optimization, smart cities, new dimensions in solar energy, the Internet of Things applications, and blockchain technology. He is a member of the International Society for Industrial Ecology (ISIE), USA. He also serves as an Associate Editor for the *International Journal of Renewable Energy and Environmental Engineering* and *Sustainable Materials and Manufacturing Process* and a Review Editor for the *Frontiers in Energy Research*. He also served as a Guest Editor for *Sustainability* journal in MDPI and a Recognized Reviewer for many peer-reviewed journals in Elsevier, IEEE, Springer Nature, MDPI, and others.